

MOHAMMED, A.I., BARTZAS, K., JOHNSON, C., SPENCE, S., SYKES, P., KIDD, G., MCCONNACHIE, J. and NJUGUNA, J. 2023. Structural response of a compliant pipe-in-pipe under frictionless and frictional conditions of the seabed. *Ocean engineering* [online], 276, article 114020. Available from: <https://doi.org/10.1016/j.oceaneng.2023.114020>

# Structural response of a compliant pipe-in-pipe under frictionless and frictional conditions of the seabed.

MOHAMMED, A.I., BARTZAS, K., JOHNSON, C., SPENCE, S., SYKES, P., KIDD, G., MCCONNACHIE, J. and NJUGUNA, J.

2023

© 2023 The Authors. Published by Elsevier Ltd. This is an open access article under the CC BY-NC-ND license (<http://creativecommons.org/licenses/by-nc-nd/4.0/>).



## Structural response of a compliant pipe-in-pipe under frictionless and frictional conditions of the seabed

Auwalu I. Mohammed<sup>a,b</sup>, Konstantinos Bartzas<sup>b</sup>, Callum Johnson<sup>b</sup>, Stuart Spence<sup>b</sup>, Paul Skyes<sup>b</sup>, George Kidd<sup>b</sup>, Jennifer McConnachie<sup>b</sup>, James Njuguna<sup>a,b,\*</sup>

<sup>a</sup> National Subsea Centre, 3 International Ave., Dyce, Aberdeen, AB21 0BH, UK

<sup>b</sup> School of Engineering, Robert Gordon University, Garthdee Road, Aberdeen, UK

### ARTICLE INFO

Handling Editor: Prof. A.I. Incecik

#### Keywords:

PIP  
Pipeline stress  
FEA  
Seabed  
Pressure  
Temperature

### ABSTRACT

Pipe-in-Pipe (PIP) technology has been studied significantly owing to its superior performance in deep-water and high-pressure high temperature fields than conventional single pipe. The PIP system has excellent track record of mitigating flow assurance problems from subsea wells through maintenance of the fluid's temperature in the pipe. It has also been applied in marine environment where conventional single pipe cannot perform. However, owing to complex interaction and contact within the PIP system and seabed, the mechanism of load transfer and the stresses that developed due to pressure, temperature and combined loading has not been fully understood and quantified. Therefore, this study examined the effect of pressure, temperature and the combined loading on PIP systems for flat seabed subsea pipeline. Simulations are performed to examine frictional and frictionless conditions of the flat seabed on PIP system and individual results of inner pipe, insulation material and outer pipe are presented for each analysis. The analytical calculations are carried-out for determining the operating stresses in each component of the PIP system in view of its significance for the overall structural behaviour of the system and validation of the numerical model. The impact response of the inner pipe, insulation and the outer pipe based on pressure, temperature and the combination of both (pressure and temperature) and the resulting stress on each component of the PIP system are investigated and the result presented. Furthermore, results of axial, radial and hoop stresses for the individual loading condition and with coupled analysis corresponding to each simulation (Frictional and Frictionless seabed conditions) are found to be closely similar with percentage difference less than 5 except for the von Mises stress which give 5.3%. This interesting finding revealed that the friction force does not affect structural integrity of the PIP system compared to conventional - single pipeline assuming all other parameters remains constant. Moreover, the presence of the outer pipe and the insulation material enhanced the performance of the inner pipe. The numerical simulation predicts closely the impact response for pipe-in-pipe composite specimens under individual and combined loading conditions. Therefore, the results obtained will serve as a reference guide for designing, construction and operating PIP system in the future to develop unconventional challenging energy resources like High Pressure High Temperature fields.

### 1. Introduction

The transportation of high-pressure high temperature (HPHT) and deep-water reservoir fluids from subsea wells is made with the use of pipe-in-pipe systems to ensure flow assurance in most cases. The PIP systems are capable of maintaining the produced hydrocarbons at temperatures well above 120 °C and pressures in excess of 10,000 psi owing to its exceptional thermal insulation and efficiency (Sriskandarajah et al., 1999; Auwalu et al., 2015; Cai and Le Grogne, 2022; Zhang

et al., 2018). This is important as it prevents wax and hydrate formations due to cooling along the length of the pipeline - hydrates are ice-like crystals that form in the pipeline where there is high pressure and low temperature (Joule-Thompson effect). Therefore, maintaining the temperature of the well fluids above the hydrate formation temperature is essential to ensure the flow of hydrocarbons. This is advantageous as otherwise costly intervention may be required when the production rate decrease notably due to flow assurance issues.

In the literature, single pipe and PIP are widely published and documented primarily covering different aspect of the pipeline system

\* Corresponding author. National Subsea Centre, 3 International Ave., Dyce, Aberdeen, AB21 0BH, UK.

E-mail address: [j.njuguna@rgu.ac.uk](mailto:j.njuguna@rgu.ac.uk) (J. Njuguna).

<https://doi.org/10.1016/j.oceaneng.2023.114020>

Received 21 October 2022; Received in revised form 29 January 2023; Accepted 17 February 2023

Available online 21 March 2023

0029-8018/© 2023 The Authors. Published by Elsevier Ltd. This is an open access article under the CC BY-NC-ND license (<http://creativecommons.org/licenses/by-nc-nd/4.0/>).

Nomenclatures			
$\sigma_{hc}$	hoop stress in the carrier pipe	$N_{vj}$	thermal force due to Poisson's effect
$p_i$	Internal operating pressure	$\sigma_{HJ}$	hoop stress jacket
$D_{co}$	Carrier pipe's outer diameter	$\sum N_T$	Total thermal force on the pipe -in-pipe system
$t_c$	Carrier pipe's wall thickness	$N_{TC}$	thermal force on carrier pipe
$\sigma_{hj}$	hoop stress outer pipe (jacket)	$N_{Tj}$	Thermal force on jacket pipe
$p_o$	External hydrostatic pressure	$\sum N_v$	summation of forces due Poisson's effect
$D_{jo}$	Jacket's outer diameter	$N_{vc}$	Force on carrier pipe due to Poisson effect
$t_j$	Jacket pipe's wall thickness	$N_{vj}$	Force on jacket pipe due to Poisson effect
$\mu_o$	reduced axial friction coefficient	$L_a$	Active length of the pipe in-system
$\mu$	Seabed longitudinal friction coefficient	$F_S$	Tie in spool frictional resistance force
$\mu_s$	Spacer friction coefficient	$L_o$	limit length
$W_c$	Weight of carrier pipe in air	$E_p$	Young's Modulus of the inner pipe
$W_{pip}$	Submerged weight of pipe in pipe	$E_c$	Young's Modulus outer pipe
$N_{TC}$	thermal force on the carrier pipe	$\Delta T_x$	Temperature distribution in the pipe-in-pipe system at 'x' distance from inlet
$A_{csc}$	Cross sectional area of carrier pipe	$K_2$	is the index of temperature decay
$E$	Young's modulus	$x$	Longitudinal direction of the pipeline
$\alpha$	coefficient of thermal expansion of the pipe	$\sigma_{Lc}$	stress in the carrier pipe when x is greater than or equal to $L_a$
$T_i$	Design temperature of carrier pipe	$\sigma_{Lj}$	stress in the jacket pipe when x is greater than or equal to $L_a$
$T_a$	Ambient temperature equal to installation temperature	$\sigma_h$	Tensile hoop stress
$N_{vc}$	force acting on the carrier pipe due to Poisson's effect	$\eta_h$	is the usage factor
$\nu$	Poisson's ratio	$\sigma_y$	is the yield stress
$N_E$	end cap force due to bulkhead	$k_t$	Temperature design factor
$A_{cin}$	Internal of the carrier pipe	$OD$	outside diameter
$p_{ans}$	Annular pressure	$t$	wall thickness
$A_{ans}$	Cross-sectional area of the annular space between carrier and the jacket pipe	$\sigma_e$	equivalent stress
$A_{jout}$	External area of the jacket pipe	$\sigma_l$	longitudinal stress
$p_e$	external pressure	$\tau$	shear stress
$N_{EC}$	Thermal expansion load	$\sigma_R$	Radial stress
$A_{csj}$	Cross -sectional area of the jacket pipe	$\sigma_{vmc}$	Von Mises stress carrier pipe
$A_{csc}$	Cross -sectional area of the carrier pipe	$\sigma_{vmj}$	von Mises stress jacket pipe
$\epsilon_{Tj}$	Thermal strain in the jacket pipe	$\sigma_{lj}$	longitudinal stress in the jacket pipe
$N_{Tj}$	Thermal force acting on the jacket pipe		

such as pipeline expansion, buckling and free span phenomena (Palmer and Ling, 1981; Choi, 2001; Zhang et al., 2018). Different approaches are adopted which included using iterative methods to solve the interaction of subsea pipeline expansion and end restraints due to thermal loads (Kershenbaum et al., 1996). For example, recent study by Gao et al. (2022) established the mechanical performance of different parts of the pipe-in-pipe specimens using experimental tests to obtain the stress-strain curves of each component. Also, Zhang and Hu (2022) study the buckling failure phenomena in liner pipe under complex loading. Rossini et al. (2012) and Gadala et al. (2016) studied the effects of thermal gradients and restraining forces in order to determine accurate pipeline design criteria. In addition, Kershenbaum et al. (1996) presented the introduction of lateral deviation and self-limiting stabilisation of a single pipeline under axial compressive loading on a resistive soil medium. However, the analysis of the expansion of pipe-in-pipe (PIP) systems was first simplified by (Harrison et al., 1997). In the follow up years, other researchers pursued in-depth understanding of the PIP system performance (Bokaian, 2004 and Sun et al., 2009b; Bhardwaj et al. 2020). Optimisation study on the design of PIP systems by Hausner and Dixon (2004) established how the top tension load on the installation vessel can be reduced. Also, Veritas (2006), Parisher and Rhea (2012) and several other studies based on analytical calculations examined PIP system in free span and three-dimensional response of a pipeline fixed at both ends, fixed at one end and pinned at the other. These studies included both hydrodynamic and impact loads and considered the external torsional moment induced by crossflow current

on a sagged pipeline section (Wang et al., 2014).

The efforts of many researchers in revealing the influence of external load or impacts on the pipe-in-pipe under transverse configurations proved three (3) failure stages due to indentation and the tolerable acceptable indentation to be less than 5% of the pipe diameter (Guo et al., 2020; Zheng et al., 2014; Odina et al., 2018; Sun et al., 2019). Liang et al. (2019) study thermal buckling of a conventional pipeline using energy method to establish relationship between temperature and the buckling height. However, Wang et al. (2021), Wang et al. (2017), Li and Liu (2020), Hong et al. (2015) examined lateral buckling of subsea pipeline based on initial imperfection. Again, a recent experimental and numerical study by Gao et al. (2022) established the impact resistance of submarine pipe-in-pipe. In a different study Mohammed et al. (2021) examined the buckling phenomena of casing pipe during shale extraction using FEA and machine learning. Liao et al. (2022) investigated the dynamics of tube with pipe-in-pipe structure during offshore drilling using drift element model. While Trapper (2022) pointed out that offshore pipeline are still being installed on a rough seafloor. Also, the study of Deng et al. (2022) proposed a new calculation method for determining stress intensity factor of submarine pipeline during earthquake. In terms of casing pipe material selection, Mohammed et al. (2022) proposed a multi-criteria material selection and ranking for pipe grade options in shale gas wells application. Furthermore, Trapper (2022) implemented analytical hierarchy process (AHP) to established lateral deformation as the most failure mode in PIP system. In a different study, effect of friction coefficient and bending displacement in flexible

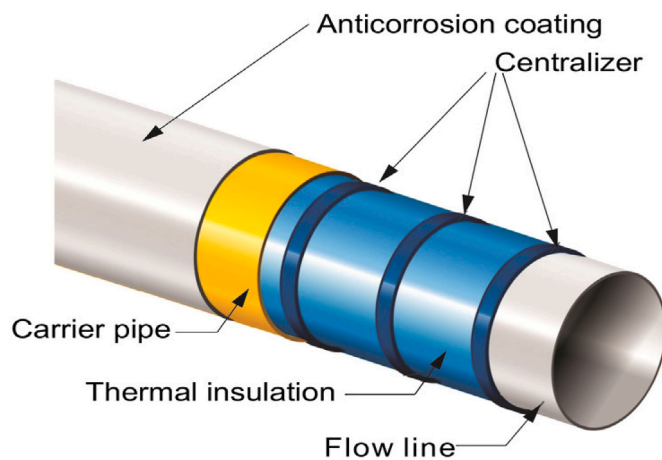


Fig. 1. Typical PIP configuration after (Bai and Bai, 2014).

pipes was established by (Provasi et al., 2022) and (Dong et al., 2017).

Park and Kim (1997) investigated the soil support at the ends of a spanned section and determined the allowable span length which limits the maximum stress in the span to within permissible limits, whilst preventing resonant oscillations due to vortex induced vibrations (VIV). Additionally, Kapuria et al. (1999) included computed rotational stiffness at the span end considering the span to be supported on an elastic soil bed, using rotational stiffness to obtain the natural frequency of the free span. Various analytical calculations are provided and compared for Pipe-in-Pipe systems in free span by Chung and Cheng (1996), Chung et al. (1995), Kristoffersen et al. (2012). Also, Giagmouris et al. (2013) presented both local and global FEA of PIP systems in free span. Sun and Jukes (2009) develop a finite element model for the installation process of PIP systems. Their follow up investigations focussed on the application of FEA for both installation and operation of PIP systems (Jukes et al., 2009). In similar studies, Sun et al. (2011) and Sriskandarajah et al. (1999) employed FEA to analyse HPHT subsea PIP pipelines and modelled buckle arrestors for PIP flowlines. In addition, the behaviour of cement filled pipe-in-pipe composite structures under transverse impact has been studied in the literature by (Wang et al., 2009). Jones et al. (2013) employed FEA for the determination of stress on pipeline during installation and demonstrated the importance of using a sleeve in comparison to a Reel-lay installation. The study showed that the non-overlapping sleeve prevents failure from buckling as it will increase the assembly's bending stiffness. Despite these efforts, the effect of pressure, temperature and combined loading on the PIP system performance considering friction and frictionless conditions has not been fully investigated and understood.

The high pressures and temperatures differentials in the PIP system will lead to the formation of a longitudinal compressive force on the inside of the pipeline. The operating stresses induced by the effective axial force will cause axial thermal expansion of the pipeline, thus the pipeline will be subjected to high axial compressive loads as established by (Zhang and Duan, 2015). In situations where the pipeline is buried under the seabed, the downward or sideways movement is restricted due to the weight of the soil. The only possible movement that can take place is upwards as the resistance exerted on the pipeline is much less compared to the downward and sideways restraint on the pipe. Under these circumstances, upheaval buckling of a subsea pipeline can occur. Upheaval buckling is a failure mode occurring from the interaction between the axial compressive force and pipeline's local curvature, putting pipeline's structural integrity at high risk, with potential catastrophic consequences.

In particular, the structural performance of a PIP system depends largely on both the overall behaviour of the system and the mechanism of load transfer between the inner and outer pipes. For example, the

effective axial stress developed in the PIP system is one hand a function of pressure and temperature. While on the other hand, the condition in which the pipeline is operating, such as seabed characteristics, the frictional forces as well as the wave and current action of sea would to a great extend affect the stresses of the PIP system. Furthermore, these stresses will vary depending on the PIP system used, that is, compliant or noncompliant and the presence of end bulkheads. Owing to these obvious complexities of the PIP system, with different factors contributing to the loads as pointed in the preceding sentences, the evolution and contribution of these loads in each component of the PIP are grossly misunderstood with loads often under-estimated leading to different kinds of failure mode of the system during design, installation and operation. Therefore, this study focuses to determine the evolution of these loads and magnitude of each on inner, insulation and carrier pipe based on temperature, pressure, combined loading of pressure and temperature with consideration of frictionless and frictional forces that evolved between the PIP system and the seabed under several scenarios. Doing this will provide a new enhance understanding of the load transfer mechanism and the stresses that developed in each component and overall structural response of the PIP system.

## 2. The PIP system

The PIP system is usually manufactured in 12–100 m m in length and comprises of a stiff steel inner pipe and a rigid outer pipe. Typically, the thickness of the carrier pipe is smaller than that of the inner pipe as it is not subjected to operating pressure and temperature. However, the outer pipe's wall thickness is of crucial importance as the water depth increases. The inner and outer pipes are separated at the ends of each joint by spacers and at the ends of the pipeline by bulkheads. The high thermal insulation of the PIP system is provided by the gap of air between the two pipes. This gap provides the necessary space to accommodate the insulation material which can be either in the form of a blanket that covers the whole outer face of the inner pipe or in the form of granular material filling completely the annulus between the two pipes (Sun et al., 2009).

Several PIP configurations have been utilised in offshore fields and factors such as the gap thickness between the two pipes, the thermal stability but also the overall feasibility must be considered for the determination of the PIP configuration. Fig. 1 presents a typical configuration of the PIP system.

In the oil and gas industry two types of PIP systems are used for offshore applications, the un-bonded PIP and the fully bonded PIP. In the former (unbonded PIP), the insulation layers of standard size are wrapped around the inner pipe whereas in the latter (fully bonded PIP) the entire space between the two pipes is filled with insulation material. This study focuses on a fully bonded PIP system where Polyurethane foam is the selected material regarding the insulation of the system (Sriskandarajah et al., 1999). The PIP systems except being categorised as un-bonded or fully bonded are also classified as compliant or non-compliant with reference to their structural behaviour, where the compliance can be determined with regard to the axial and bending response. The main difference that distinguishes the two categories is based on the method by which the load is transferred between the inner and outer pipe. A continuous load transfer between the two pipes along the length of the pipeline characterises the compliant systems whereas non-compliant systems are defined as those where the load transfer takes place at discrete locations (Sriskandarajah et al., 1999).

### 2.1. PIP performance

The two main reasons for the utilisation of such systems are the existing harsh reservoir conditions and the requirement for flow line insulation which will not allow the cooling of the well fluids along the pipeline in cold marine environment. Due to the extraordinary thermal insulation of pipe-in-pipe systems; formation of hydrates or wax can be

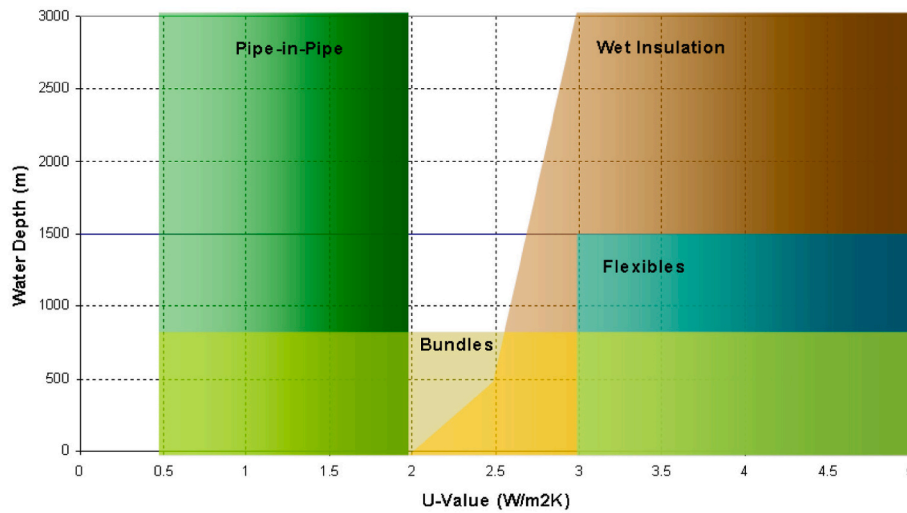


Fig. 2. Shows the performance of PIP, Pipe Bundles, Flexibles, and Wet Insulation based on water depth and thermal conductivity. After (Watson and Walker, 2012).

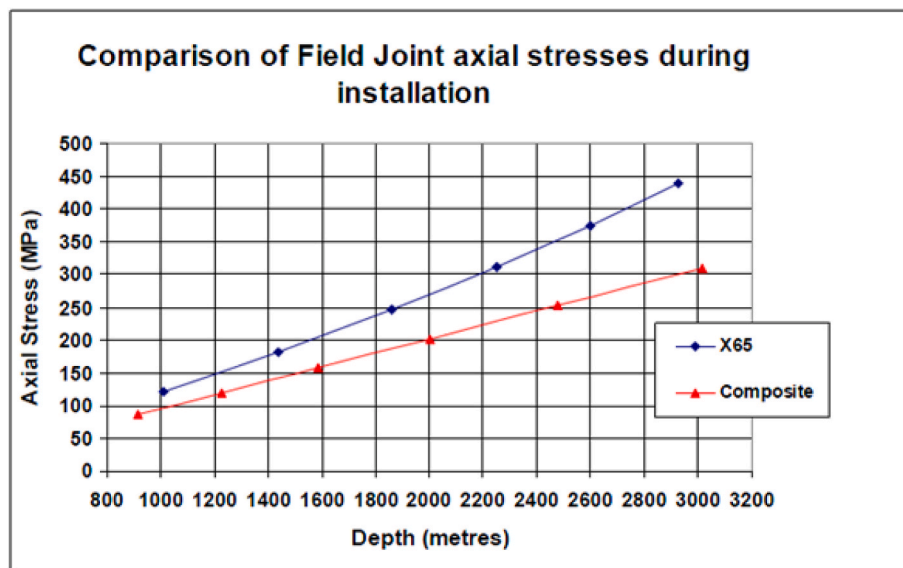


Fig. 3. PIP hang off axial stress comparison (Jones et al., 2013).

prevented, the high arrival temperature at the production facilities is ensured and the impact on flow assurance is mitigated, averting a complete shutdown. Fig. 2 presents the operating boundaries (water depths) versus thermal conductivity coefficients of PIP, Flexibles, Bundles and Wet insulation as shown.

Another advantage of the PIP system is its reliability and efficiency in the transportation of large quantities of fluids on daily basis with an excellent safety record and cost effectiveness. The original capital expenditure (CAPEX) may be substantial to design, fabricate and install the PIP pipeline system. However, the operating expenditure (OPEX) is minimal compared to their alternatives such as hiring large oil tankers and floating storage and offloading (FSO) vessels with expensive day rates. The advantage of using pipelines mainly owes to the fact that they are unaffected by weather conditions and can operate at the same flow rates all year round (Adegboye et al., 2019; Kong et al., 2020).

Even though a pipe-in-pipe system can provide low values of thermal conductivity, its increased weight in relation to a single pipe, is an important disadvantage which raises the manufacturing cost and makes its installation challenging in deep water environments as noted by (Bayart et al., 2007). The weight of the PIP systems can be a concern

during installation especially for conventional installation methods in water depth greater than 7000 ft (2133.6m) as pointed by (Bayart et al., 2007). The weight of the PIP system over such a water depth can cause severely high axial stresses. This results in either the installation vessels having to be modified to reduce the hang-off weight or using different materials to reduce the system weight. One method proposed by Jones et al. (2013) is to create the outer pipe with composite materials which are lighter and installable using current installation methods as they possess sufficient strength to operate safely in water depths up to 9843 ft (3000 m) (Jones et al., 2013). Moreover, PIP system with a composite outer pipe suffers less axial stress than those made of API 5L X65 steel as shown in Fig. 3 (Jones et al., 2013).

### 3. Theoretical modelling

As pointed earlier in the introduction, the load transfer and the structural performance of the PIP System is based on the compliant or noncompliant and the local operating conditions of the seabed and the pipe physical properties. However, regardless of these factors and the circumstance in which the pipe is installed and operated, one form of

stress or the other exist in the PIP system depending on the configuration, installation and the operation (Mohammed et al., 2019). Therefore, a detail understating of the load transfer due to thermal, pressure and friction forces and their corresponding stresses on each of the component is paramount to improve structural performance in the future designs, installation and operation. For completeness, the underlying theoretical modelling is provided in subsections 3.1, 3.2 and 3.3.

### 3.1. Hoop stress in the PIP system

A pipeline that is buried or unburied, in both cases has an active part and a fully restrained part. In the event of a subsea buried pipeline, the large contact area with the seabed is responsible for restraining most of the pipeline section due to a combination of friction and soil pressure. The possibility of expansion is mitigated as a buried pipeline presents minimum movement even under high pressure and temperature. On the other hand, operations regarding burial of pipelines are difficult and expensive, and that lead to the development of unburied pipeline designs. The mobility of an unburied pipeline is increasing due to low contact area with the sea bottom and that may permit significant axial elongation and lateral divergence (Harrison et al., 1997).

A subsea PIP system is under thermal expansion due to transportation of hot production fluids from the subsea wells. As a result, high pressure and temperature cause pipeline expansion which is defined by a number of factors such as the thermal expansion coefficient, Poisson's ratio, internal pressure, seabed conditions and the forces that interact between the jacket (outer pipe) and carrier pipe. The carrier pipe expands but the expansion is restricted due to friction forces from centralisers, the shrinkage of Poisson's ratio and the reaction of jacket pipe at bulkheads and spacers (Harrison et al., 1997). The first establishment of a simple analytical method for a pipe in pipe system is reported by Harrison et al. (1997) on their expansion in subsea environment. The hoop stress in the carrier pipe (inner pipe) is due to internal pressure only and hoop stress in the jacket pipe is due to external pressure only. Hence,  $\sigma_{hc} = \frac{p_i D_{co}}{2t_c}$  where  $\sigma_{hc}$  hoop stress in the carrier pipe and  $p_i$  Internal operating pressure,  $D_{co}$  Carrier pipe's outer diameter,  $t_c$  Carrier pipe's wall thickness. Then, the value of hoop stress in the outer pipe can be estimated as  $\sigma_{hj} = \frac{p_o D_{jo}}{2t_j}$  where  $p_o$  is the external hydrostatic pressure,  $D_{jo}$  is jacket pipe's outer diameter and  $t_j$  is the Jacket pipe's wall thickness

### 3.2. Longitudinal stress

The longitudinal stress in the carrier and jacket pipe can be determined as long as the active length of the pipeline is known. The active length of the pipeline can be estimated with the use of formulae presented by Bokaian (2004) in his work regarding an extensive mathematical model for the thermal expansion of pipe in pipe systems. In order to calculate the value of the PIP's active length, the determination of certain parameters is required such as the reduced longitudinal seabed friction coefficient and the tie-in spool piece frictional resistance force, the end cap force, but also the forces in the inner and outer pipe due to Poisson's and thermal effects. The following equations are based on the assumption that the temperature along the length of the PIP system is distributed uniformly. The equation describing the reduced longitudinal seabed friction coefficient is given as  $\mu_o = \mu \left( 1 - \frac{\mu_s}{\mu} \frac{W_c}{W_{pip}} \right)$  where  $\mu$  is the seabed longitudinal friction coefficient,  $\mu_s$  is the spacer friction coefficient,  $W_c$  is the weight of carrier pipe in air and  $W_{pip}$  is submerged weight of pipe in pipe (Bokaian, 2004).

The value of the thermal force on the carrier pipe can be estimated by using equation  $N_{TC} = EA_{csc} \alpha (T_i - T_a)$  where  $E$  = Young's modulus,  $A_{csc}$  = cross sectional area of carrier pipe,  $T_i$  = design temperature of carrier pipe and  $T_a$  = ambient temperature equal to installation temperature. Next, the force acting on the carrier pipe due to Poisson's effects can be calculated with the use of equation  $N_{vc} = \sigma_{HC} A_{csc} \nu$  with the estimation of

the end cap force value on the bulkhead can be calculated as  $N_E = (p_i A_{cin}) + (p_{ans} A_{ans}) - (p_o A_{jout})$  where  $p_i$  = inner pipe design pressure,  $A_{cin}$  = Internal area of carrier pipe,  $p_{ans}$  = Annulus pressure equal to atmospheric pressure,  $A_{ans}$  = Annular area between carrier and jacket pipe, and the  $A_{jout}$  = External area of jacket pipe. The end cap force on the bulkhead, shared by both the carrier and jacket pipes proportional to the axial stiffness, can be evaluated as  $N_{EC} = \frac{EA_{csc}}{EA_{csc} + EA_{csj}} N_E$  where  $E$  = Young's modulus and  $A_{csj}$  = Cross sectional area of the jacket pipe. The end cap strain can be estimated as  $\epsilon_E = \frac{N_E}{E_p A_{csc} + E A_{csj}}$ . If the jacket pipe's temperature is increased due to heat convection from the carrier pipe, the thermal strain in the jacket pipe can be calculated using  $\epsilon_{Tj} = \alpha (T_{dj} - T_a)$ .

The value of the thermal force acting on the jacket pipe can be estimated in the following  $N_{Tj} = EA_{csj} \epsilon_{Tj}$ . Also, the force acting on the jacket pipe due to Poisson's effects can be calculated as  $N_{vj} = -\nu \sigma_{hj} A_{csj}$ . The total thermal force acting on the pipe in pipe system can be calculated by summarising the thermal forces on the carrier and jacket pipe respectively leading to  $\sum N_T = N_{TC} + N_{Tj}$ . Hence, the sum of the forces due to Poisson's effects can be calculated as  $\sum N_v = N_{vc} - N_{vj}$ .

A static point at the centre of the pipe in pipe system is localised due to the assumption that the system has two identical tie-in spool pieces. As a result of the force equilibrium, equation (1) is used for calculating the active length of the pipe in pipe system.

$$L_a = \frac{L}{2} \frac{-1 + \sqrt{1 + 4 \left( \frac{\mu_s W_{cl}}{2 \mu_o L W_{pip}} \sum N_T + N_E - F_s \right) \frac{E_c A_{sj}}{E_p A_{sc}}}}{\frac{E_p A_{sc}}{E_c A_{sj}}} \quad (1)$$

where  $L_a$  = Active length of the pipe in pipe system and  $F_s$  = Tie in spool frictional resistance force. In order for the formula describing the active length to be valid the following three conditions are requisite: (i) The value of active length has to be limited between  $0 < L_a \leq L/2$ ; (ii) the tie in spool frictional resistance must meet the inequality i.e.,  $F_s \leq \sum N_T - \frac{\mu_s W_{cl}}{2} - \sum N_v + N_E$  and The limit length between short and long pipe in pipe systems, is symbolised as  $L_o$  and must meet the inequality  $L \geq L_o$  where  $L$  is the length of the pipe in pipe system.

The value of the limit length between short and long pipe in pipe systems can be estimated using the following equation.

$$L_o = \frac{1}{\mu_o W_{pip}} \left( \frac{E_c A_{sj}}{E_p A_{sc}} \right) \left( -\sum N_T - \sum N_v + N_E - F_s \right) \frac{1}{0.25 + \left( \frac{E_c A_{sj}}{2 E_p A_{sc}} \right) \left( 1 + \left( \frac{\mu_s}{\mu_o} \right) \left( \frac{W_c}{W_{pip}} \right) \right)} \quad (2)$$

In case where the value of  $L_o$  is smaller than the value of  $L$  the pipe in pipe system is considered as short and as a result the longitudinal seabed friction affects the whole length of the system.

The pipeline expansion due to thermal loading can be defined by the following equation.

$$\Delta L_t = \alpha \int_0^{L_a} \Delta T_x dx = \frac{\alpha (T_i - T_a)}{K_2} (1 - e^{-K_2 L_a}) \quad (3)$$

where  $x$  = Longitudinal direction of pipeline,  $K_2$  = Index of temperature decay;  $K_2 = \frac{U}{C_p \rho Q}$  and  $\Delta T_x$  = Temperature distribution in the pipe in pipe system at  $x$  distance from the inlet is  $\Delta T_x = T_x - T_a = (T_i - T_a) e^{-K_2 x}$ . The values of longitudinal stresses both in the carrier and jacket pipe can be estimated considering the inequality equations between the active length and the longitudinal direction of pipeline. In case where  $x \geq L_a$  then the equations describing the longitudinal stress in the carrier and jacket pipe are shown as  $\sigma_{Lc} = -\alpha E \Delta T_x + \nu \frac{D_{co}}{2t_c}$  and  $\sigma_{Lj} = \nu \frac{D_{jo}}{2t_j}$ .

### 3.3. Von Mises

Depending on the considered design case, limitations of stresses to some fraction of the SMYS apply. Based on the equivalent and hoop

**Table 1**  
Summary of the PIP simulation carried out.

System	Friction	Loading Condition	Pressure Internal/External	Temperature Internal/External
PIP	Frictionless	Pressure	64.13 MPa/ 14.48 MPa	–
	Frictionless	Thermal	–	120.15 °C/4.444 °C
	Frictionless	Pressure + Thermal	64.13 MPa/ 14.48 MPa	120.15 °C/4.444 °C
	Frictional	Pressure + Thermal	64.13 MPa/ 14.48 MPa	120.15 °C/4.444 °C

**Table 2**  
Materials and dimensions.

	Inner/Outer Pipe	Insulation	Seabed
Material	API 5L X65		
Elastic Modulus (E)	207 000 MPa	75.84M Pa	50 MPa
Poisson's Ratio (ν)	0.3	0.3	0.4
Coefficient of Thermal Expansion (α)	1.16 × 10 <sup>-5</sup>	–	–
Thermal Conductivity (U)	50W/m.K	0.0007W/m.k	0.975W/m.k
Density (ρ)	7850 kg/m <sup>3</sup>	100 kg/m <sup>3</sup>	1500 kg/m <sup>3</sup>
Friction Factor (Relative to Pipeline)	–	0.3	0.4
Outer Diameter (mm)	304.80/406.60	362.9	–
Inner Diameter (mm)	362.90/269.80	304.8	–
Wall Thickness (mm)	21.85/17.50	29.05	–
D/t Ratio	18.60/17.42	12.49	–

stress criteria, two checks have to be carried out. The tensile hoop stress to a fraction of SMYS due to internal overpressure is given below as:  $\sigma_h = \eta_h \cdot \sigma_y \cdot k_t$  where  $\eta_h$  = is usage factor,  $\sigma_y$  = Yield stress and  $k_t$  = Temperature design factor. Calculation of hoop stress according to thin wall theory is given by Barlow formula as  $\sigma_h = \frac{(p_i - p_e)}{2t} OD$  where  $p_i$  = Internal pressure,  $p_e$  = External pressure,  $OD$  = Outside diameter and  $t$  = Wall thickness, whereas the von Mises or Tresca yield criteria provide the limitations for the combined stress criterion.

For values of D/t ratio higher than twenty, the equivalent stress in its biaxial form can be estimated and the expression of the criterion is given as  $\sigma_e = \sqrt{\sigma_h^2 + \sigma_l^2 - \sigma_h \sigma_l + 3\tau^2} \leq \eta_e \eta_y$ . In case of pipes where high pressures are present and the D/t ratio is less than twenty, the equivalent stress in its triaxial form should be estimated and the von Mises criterion below should be used since  $\sigma_e = \sqrt{\frac{1}{2}[(\sigma_h - \sigma_l)^2 + (\sigma_l - \sigma_R)^2 + (\sigma_h - \sigma_R)^2]}$ . The determination of wall thickness in order to meet the hoop stress criteria is the most common method for designing pipelines. Following satisfaction of the hoop stress criteria, the equivalent stress criteria for both hoop and axial stress in terms of temperature, pressure and bending can be satisfied. Although this method is acceptable for pipelines operating at temperatures below 100 °C, it presents major limitations regarding flow lines that operate at high temperatures. The attempt of satisfying the combined stress criterion for high temperature pipelines, leads to limitation capacity of hoop stress due to internal pressure as established by (Sriskandarajah et al., 1999).

The Von Mises stress both for the carrier and jacket pipe can be determined taking the following form for each case individually.

$$\sigma_{vmc} = \sqrt{\frac{1}{2} [(\sigma_{hc} - \sigma_{lc})^2 + (\sigma_{lc} - \sigma_R)^2 + (\sigma_{hc} - \sigma_R)^2]} \tag{4}$$

$$\sigma_{vmj} = \sqrt{\frac{1}{2} [(\sigma_{hj} - \sigma_{lj})^2 + (\sigma_{lj} - \sigma_R)^2 + (\sigma_{hj} - \sigma_R)^2]} \tag{5}$$

**4. Numerical modelling**

The modelling approach which examined frictionless and frictional contact in this study is summarised as shown on Table 1. The dimensions and the material's properties of the PIP pipeline, including the inner/outer pipe and insulation material are shown in Table 2. Half symmetry is used in the analysis in order to improve computational efficiency. The dimensions used for the flat seabed is shown in Fig. 4, while the thickness for the seabed in this analysis is 2 mm, in order to ensure correct contact as the analysis is three dimensional.

For ease of modelling, the PIP system, including the inner and outer pipes and the insulation, were created using Solidworks CAD software.

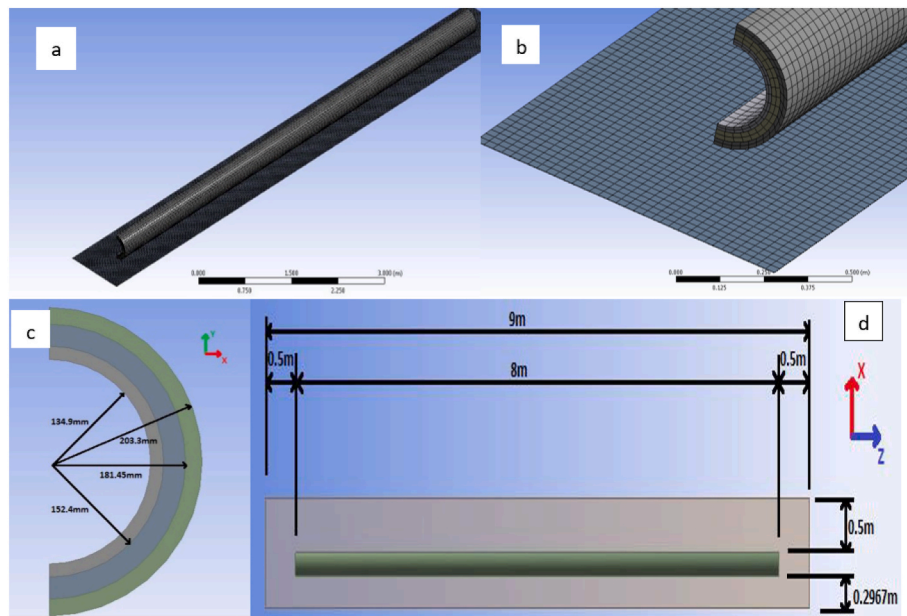


**Fig. 4.** Finite element Model (a) Global mesh (b) Scaled mesh (c) Inner Pipe, Insulation and outer Pipe (d) Flat Seabed – Seabed Geometry.

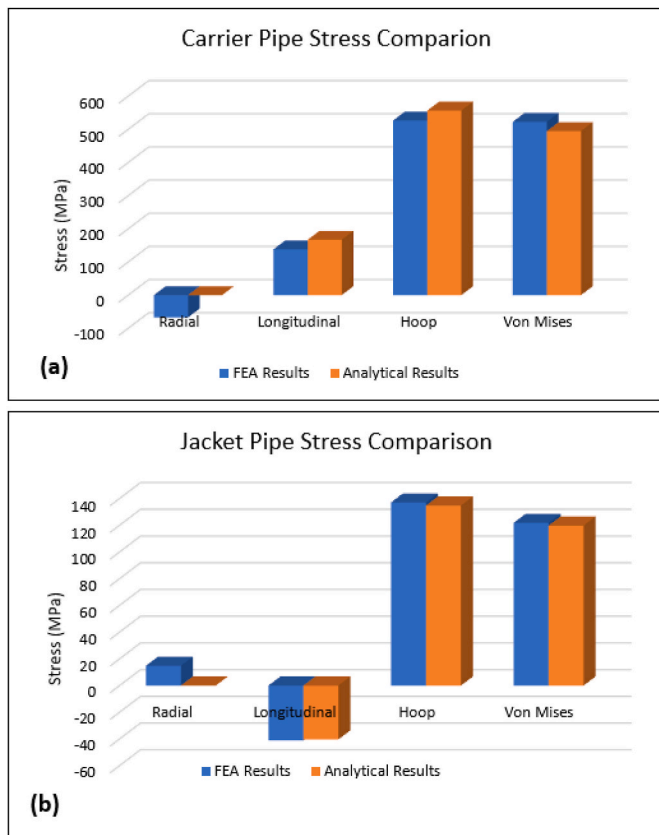


Fig. 5. Stress comparison between FEA and Analytical result (a) for carrier pipe (b) for jacket pipe.

#### 4.1. Boundary conditions

The constraint on the pipeline is applied such that the Pipeline's Z-Axis is in the longitudinal direction. A displacement ( $Z$ -axis = 0) was applied to the end faces of the pipeline. This is because the modelled section is only one short section of the much larger pipeline and therefore the overall pipeline would constrain the movement of the short section. The Pipeline Y-Axis correspond to vertical/radial/Seabed with a remote displacement applied to the face(s) of the seabed which are fixed in all directions, including rotational, providing the Y-axis constraint on the pipeline also. Finally, Pipeline X-Axis (Horizontal Radial) is a symmetry region provides the X-axis constraint which was applied to the cut off of the half symmetry model.

The contact settings used in this study are as follows. For the frictionless models, a frictionless contact is applied between the outer face of the outer pipe and the seabed. A Bonded contact region is used between the insulation and inner/outer pipes. The frictionless boundary condition applied between the inner pipe and insulation material.

In the frictional models however, frictional contacts exist between the outer surface of the outer pipe and the seabed, the outer surface of the insulation and the inner surface of the outer pipe and also the inner surface of the insulation and outer surface of the inner pipe. In all of the above cases studied, the behaviour is set to symmetric in order to aide convergence, the formulation is set to augmented Lagrange, the detection method is set to nodal-normal from contact and the interface treatment is set to adjust to touch.

A frictional surface-to-surface contact region between the outer surface of the outer pipe and the seabed, with a friction factor of 0.4 is utilised. A further two frictional surface-to-surface contact regions are used between the outer/inner pipes and the insulation, these include a friction factor of 0.3. The friction coefficient between the outer pipe and seabed is taken as 0.4. The justification for this value is established for

cohesive clays in the North Sea which varies from a minimum of 0.3 to a maximum of 1.0 in the axial configuration (Bai and Bai, 2014).

The Pressure, and thermal loading applied to the various models as tabulated in Table 1. Pressure loads are applied in the static structural analysis system in ANSYS Workbench. Pressure loading consists of: Internal operating pressure of 64.13 MPa (9.3ksi) applied to the inner faces of the pipeline. External hydrostatic pressure of 14.48 MPa (2.1ksi) applied to the outer faces, which corresponds to a water depth of 4700 ft subsea.

The thermal loading applied to the relevant models, using the steady-state thermal analysis system in ANSYS Workbench is as follows: Initial as laid internal temperature of 277.594 K (4.444 °C). External operating temperature also equal to 277.594 K (4.444 °C). Internal operating temperature equal to 393.15 K (120.15 °C).

The constraints used in this model are described earlier on, concerning the pipe-in-pipe on flat seabed models and for the pressure loading only. Mesh convergence study was performed in order to achieve accurate results. Based on the mesh sensitivity study; the mesh converges with an element length of 0.03m applied to the bodies of the inner pipe, insulation and outer pipe and also the face of the seabed. The number of elements and nodes used in this model (Fig. 4(a)) has 199669 nodes, 72198 elements, 39571 solid elements and 101572 total elements.

#### 5. Analytical results, verification and validation

The analytical expressions described in this study are used to compute pertinent stresses in the PIP systems and effect of pressure, temperature, soil cohesion and combine effect of pressure and temperature. The analytical results are related to the scenario of PIP lying on a flat seabed, which are compared with the finite element analysis results for verification and validation.

##### 5.1. Effect of pressure on PIP stresses

In the event of a PIP lying on a flat seabed, the principal stresses result due to pressure loading are calculated with the use of equations described in this study. The comparison between analytical stress results and the corresponding FEA stress results mentioned above, is essential for verification of the FEA model. However, further evaluation of differences is presented on Fig. 5 as shown. From the comparison on Fig. 5, it can be observed that the deviation percentage differences between the FEA results/analytical results show high level of accuracy with disparity less than 2% in each of the case investigated. The radial stress values according to analytical results are equal to zero both in the carrier and jacket pipe, whereas the radial stress values deriving from the FEA analysis are low (67.30 and 14.79 MPa), verifying the analytical results. The hoop stress on Fig. 5(a) as can be noted, the maximum occurs on the carrier pipe, where the hoop stress acts in a tension (positive). In contrast, Fig. 5(b) presents the minimum values on the jacket pipe where the hoop stress acts compressively (negative) due to the external pressure exerted on the outer pipe.

The hoop stress on the inside of the carrier pipe is affected by the internal operating temperature, where its value is decreasing progressively as is carried through the insulation to the jacket pipe. In the same way it can be noticed that the axial (longitudinal) stress is higher on the carrier pipe and lower on the jacket pipe with the stress behaviour being tensile and compressive, respectively. In addition, the Von Mises stress are three to four times greater on the carrier pipe in comparison to the outer pipe as a result of the high difference between the axial and hoop stress on the carrier and jacket pipe.

##### 5.2. Effect of temperature on PIP stresses

In the case of a PIP on a flat seabed, the principal stresses due to thermal loading are estimated with the use of equations described in this

**Table 3**  
Effect of temperature PIP/FEA-analytical results comparison.

Stress (MPa)	Carrier Pipe			Jacket Pipe		
	FEA Results	Analytical Results	(%) Deviation	FEA Results	Analytical Results	(%) Deviation
Radial	-0.45	0	N/A	0.85	0	N/A
Hoop	-3.74	0	N/A	0.85	0	N/A
Longitudinal	-278.97	-277.833	0.408	0.84	0	N/A
Von Mises	277.15	277.833	0.246	3.11	0	N/A

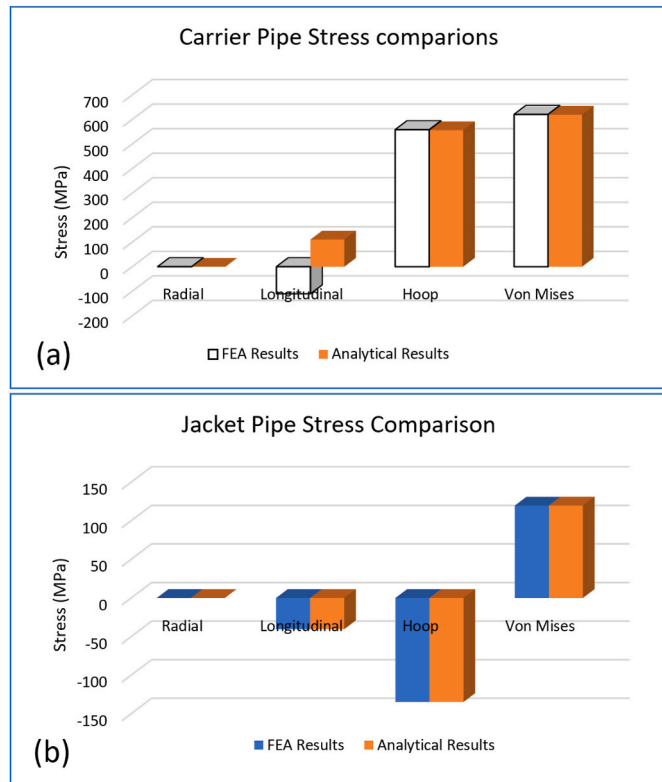


**Fig. 6.** Stress comparison due to combined loading of pressure and temperature (a) carrier pipe (b) jacket pipe.

study. The comparison between the analytical results and the corresponding FEA stress results proves the effectiveness and the accuracy of the FEA model. In similar manner, the percentage deviation between these results based on thermal loading in the PIP system is summarised on Table 3.

In Table 3 it can be seen that the radial stress according to analytical results are equal to zero both in the carrier and jacket pipe, whereas the radial stress obtained from the FEA calculation are low, verifying the analytical results. In this same way, the hoop stresses resulting from the effect of temperature loading are zero based on the analytical calculations, while on the other hand, the negligible values occurring by the FEA, confirm the validity of analytical solution. The higher axial stresses are in the carrier pipe acting in compression (negative sign). In contrast the axial stress in the jacket pipe is zero or presents a very small value corresponding to a tensile stress in the case of FEA. The Von Mises stress results on the carrier pipe correlate very well with analytical study results' which are almost equal to those obtained from the FEA solution with a deviation less than 0.5% as shown on Table 3.

5.3. Effect of combined loading (pressure and temperature) on PIP stress

In the event of the pipe-in-pipe lying on a flat seabed, the principal stresses result due to pressure and temperature effect are estimated with the use of equations described in this study. The comparison between the calculated stresses in both carrier and the jacket pipe are presented on Fig. 6. It can be observed that the FEA and analytical calculation agree very well as evidenced on Fig. 6.

The comparison between analytical stress results and the corresponding FEA stress results shows a very strong agreement between the two approaches. This essentially justify the verification of the FEA model.

According to the values of radial stresses for both the carrier and jacket pipe are considered due to assumption to be zero, while the radial stress values deriving from the FEA are low, since the effect of

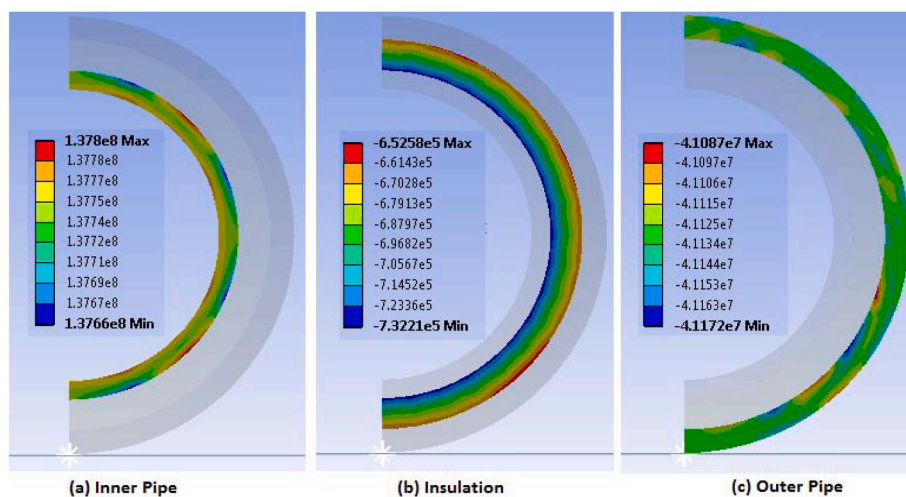


**Fig. 7.** FEA results for frictionless pipe-in-pipe on a flat seabed, subjected to pressure loading in terms of axial stress in the (a) inner pipe; (b) insulation and (c) outer pipe – units in Pa.

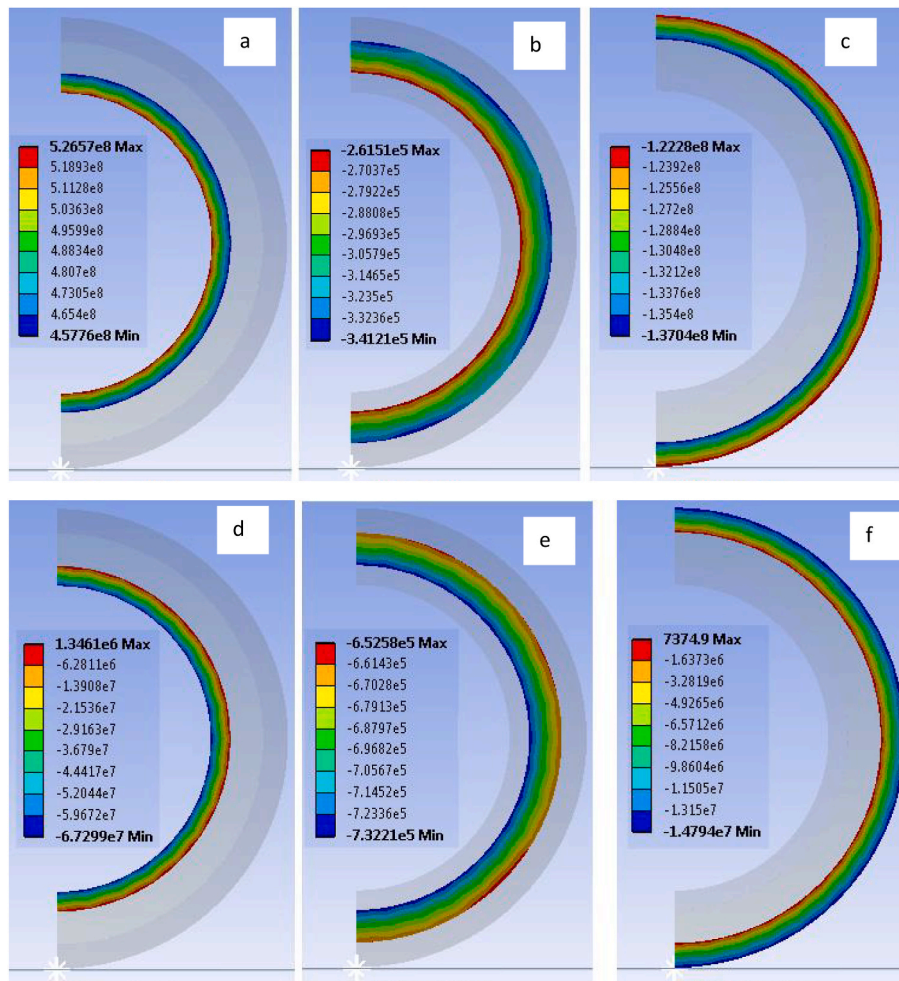


Fig. 8. FEA results for frictionless pipe-in-pipe on a flat seabed, subjected to pressure loading for hoop stress in the (a) inner pipe; (b) insulation and (c) outer pipe (d) radial stress in the inner pipe; (e) radial stress in the insulation and (f) radial stress in the outer pipe – units in Pa.

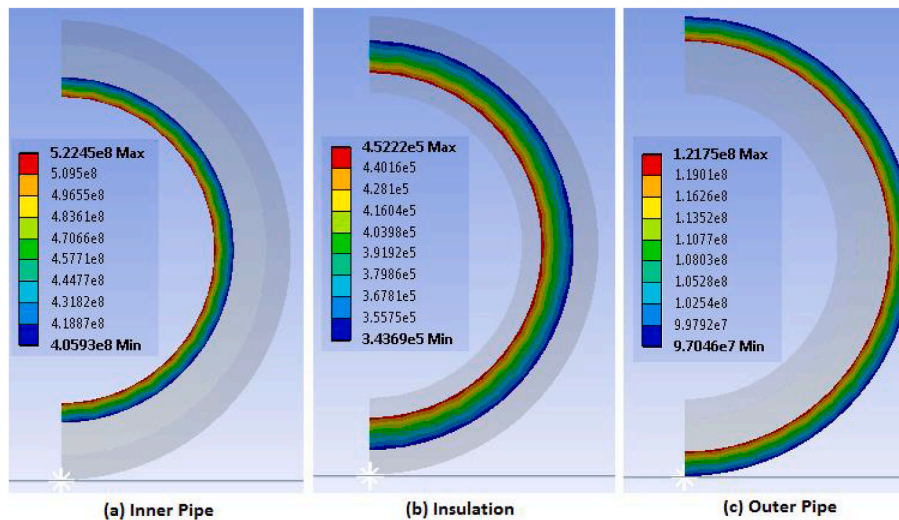


Fig. 9. FEA results for frictionless pipe-in-pipe on a flat seabed, subjected to pressure loading in terms of von-Mises stress in the (a) inner pipe; (b) insulation and (c) outer pipe – units in Pa.

temperature does not affect the radial stress magnitude, validating the analytical results. In the same way the FEA/analytical results indicate that the hoop stress in the carrier pipe is tensile while in the jacket pipe

compressive and though the deviation percentages are slightly increased, are considered acceptable since the percentage difference is below 1%. Regarding the axial stress results, it can be noticed that both

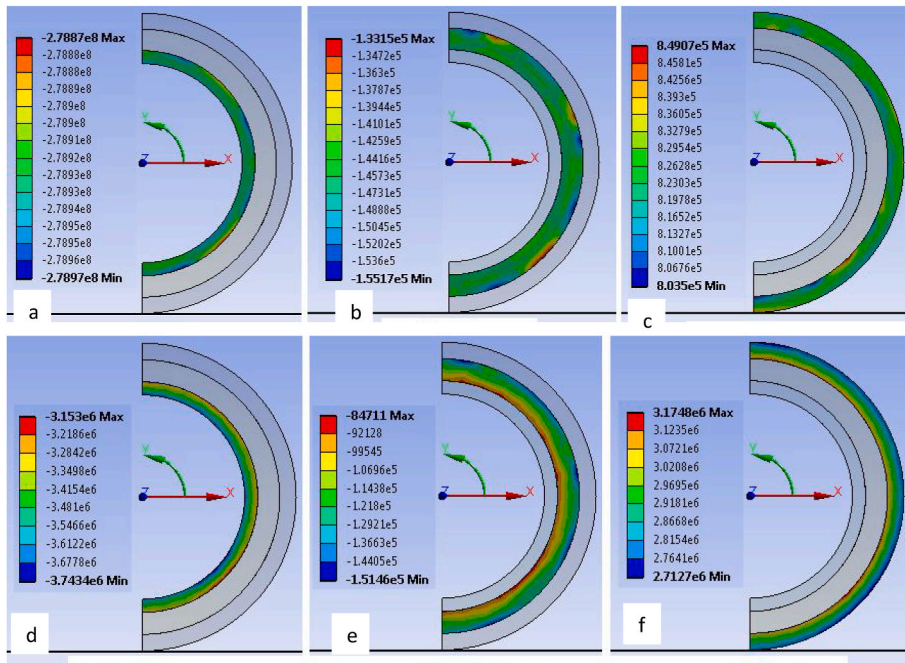


Fig. 10. FEA results for frictionless pipe-in-pipe on a flat seabed, subjected to thermal loading in terms of axial stress in the (a) inner pipe; (b) insulation and (c) outer pipe (d) hoop stress in the inner pipe; (e) hoop stress in the insulation and (f) hoop stress in the outer pipe – units in Pa.

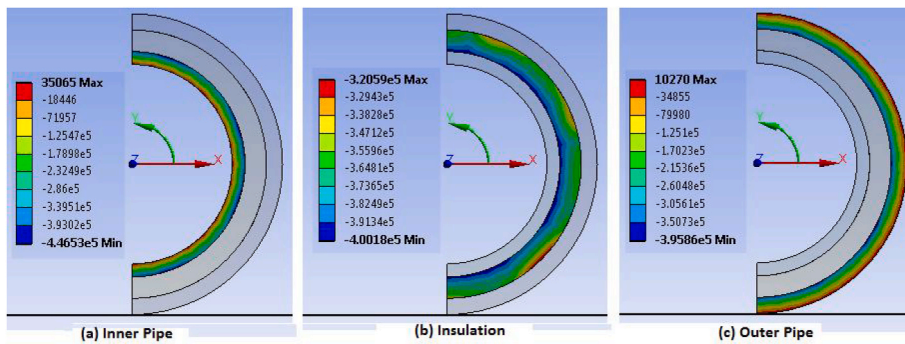


Fig. 11. FEA results for frictionless pipe-in-pipe on a flat seabed, subjected to thermal loading in terms of radial stress in the (a) inner pipe; (b) insulation and (c) outer pipe – units in Pa.

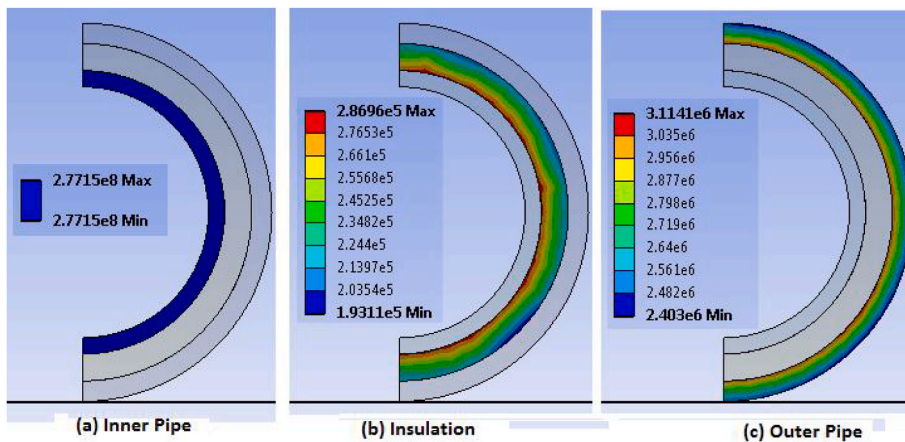
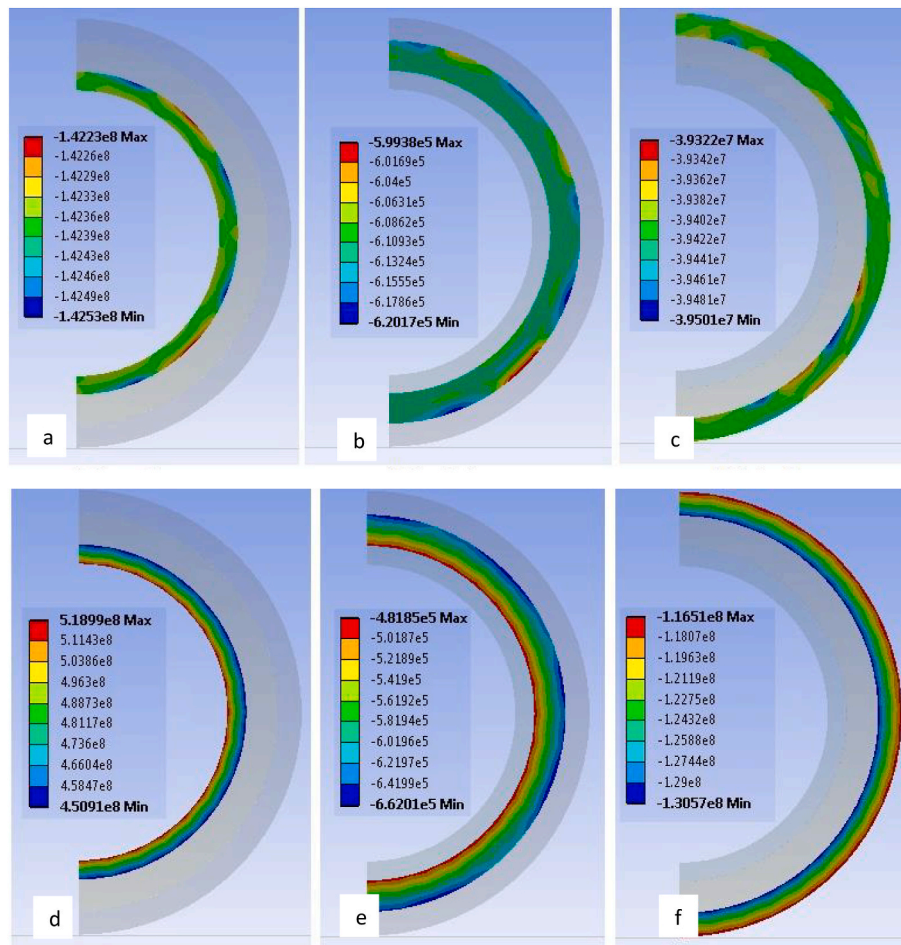


Fig. 12. FEA results for frictionless pipe-in-pipe on a flat seabed, subjected to thermal loading in terms of von-Mises stress in the (a) inner pipe; (b) insulation and (c) outer pipe – units in Pa.



**Fig. 13.** FEA results for frictionless pipe-in-pipe on a flat seabed, subjected to pressure and thermal loading in terms of axial stress in the (a) inner pipe; (b) insulation and (c) outer pipe (d) hoop stress in the inner pipe; (e) hoop stress in the insulation and (f) hoop stress in the outer pipe – units in Pa.

in the carrier and jacket pipe the stress acts compressively, presenting greater values in the carrier pipe. The Von Mises stresses results indicate that the combined stress exerted to the carrier pipe is significantly higher owing to the influence of the combined loading.

**5.4. Effect of pressure loading on PIP stresses: frictionless condition**

The results of this analysis for the axial stress in the inner, outer pipe and also the insulation, are shown in Fig. 7. It is clear from this that the maximum stress occurs on the inner surface, with a value of 137.8 MPa and the minimum value is on the outer surface, at 137.6 MPa. Similarly, on the insulation, minimal stresses are calculated, with maximum and minimum values of  $-0.732$  MPa and  $-0.653$  MPa respectively. The outer pipe has a reasonably constant through-wall stress profile, with maximums and minimums of  $-41.172$  MPa and  $-41.087$  MPa respectively, which accounts for the seemingly erroneous stress profile seen in Fig. 7(c).

The hoop and radial stresses on the other hand for PIP system, acting on each body is presented in Fig. 8. It is clear from these results that the hoop stress in the inner pipe varies from 526.57 MPa at the inner surface to 457.76 MPa at the outer surface (decreasing outward). The insulation has relatively low hoop stresses,  $-0.34$  MPa on the outer surface to  $-0.26$  MPa at the inner surface as shown on Fig. 8(b). Finally, the outer pipe ranges in values for hoop stress from  $-122.28$  MPa at the outer surface to  $-137.04$  MPa at the inner surface Fig. 8(c).

Fig. 8(d–f) presents FEA results for frictionless pipe-in-pipe on a flat seabed, subjected to pressure loading. The radial stresses vary in the inner pipe from a maximum compressive stress at the inner surface equal

to  $-67.299$  MPa to a minimum at the outer surface equal to  $1.346$  MPa Fig. 8(d). Fig. 8(e) shows that the insulation again has relatively low values for radial stress, equal to  $-0.653$  MPa at the outer surface, to  $-0.732$  MPa at the inner surface. In terms of the outer pipe, the stress at the inner surface is equal to  $7374.9$  Pa and at the outer surface is equal to  $-14.794$  MPa as shown on Fig. 8(f).

Finally, results on Fig. 9 shows that the von-Mises stresses for the inner pipe, as presented on Fig. 9(a) has a maximum von-Mises stress value at the inner surface, equal to 522.45 MPa. The minimum value of von-Mises stress in the inner pipe occurs on the outer surface which equal to 405.93 MPa as shown in Fig. 9(a). The results for the insulation material is shown on Fig. 9(b), the von-Mises stress in this instance ranges from 0.452 MPa at the inner surface, to 0.344 MPa at the outer surface. Fig. 9(c) shows that the maximum stress in the outer pipe occurs at the inner surface, a value of 121.75 MPa and varies towards the outer surface with a minimum value of 97.046 MPa.

The hoop stress in the inner pipe is tensile and largest in the inner pipe; in the outer pipe however, the hoop stresses are compressive, this is shown in Fig. 9(a–c). This is because the hoop stresses in each pipe are due to the pressures acting on that pipe individually. The inner pipe is affected by the inner operating pressure, which accounts for the tensile hoop stress seen in this pipe. This factor also causes the hoop stress to be greatest at the inner surface of the inner pipe, reducing through the wall thickness towards the outer surface. In the outer pipe, the external hydrostatic pressure, is significant, therefore the stress is compressive. Similarly, the greatest hoop stress occurs on the inner surface of the outer pipe, reducing through the wall thickness towards the inner surface. The operating pressure is greater than the hydrostatic pressure and

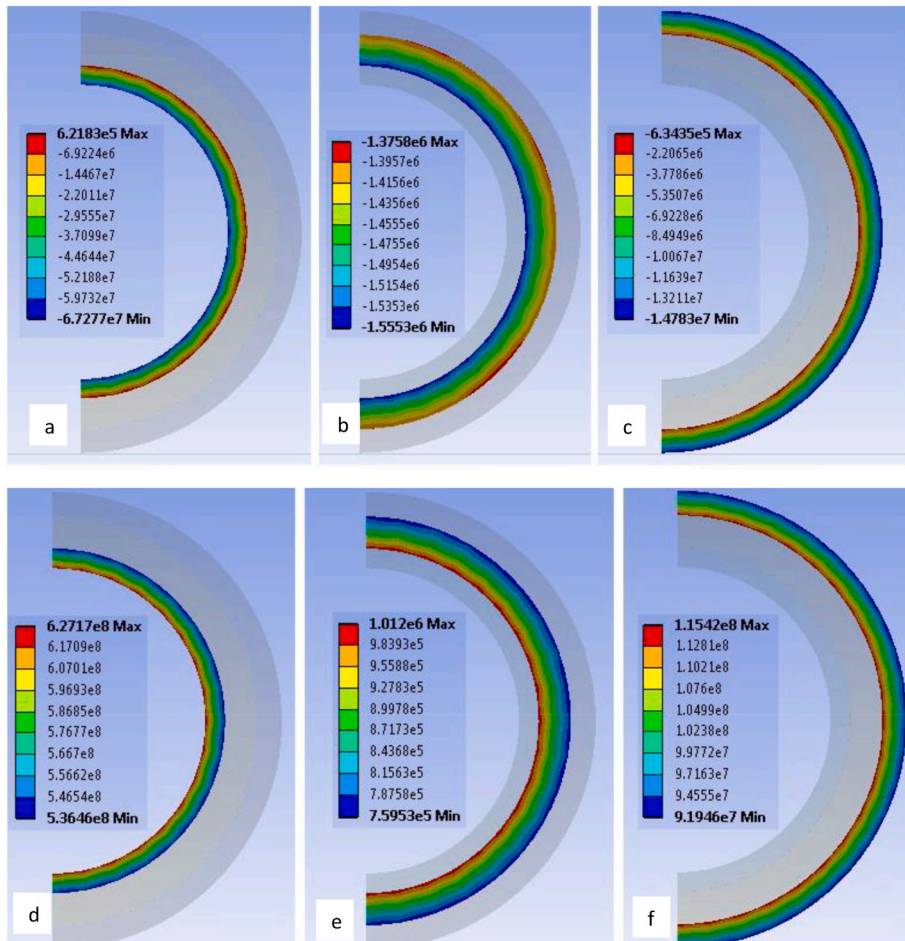


Fig. 14. FEA results for frictionless pipe-in-pipe on a flat seabed, subjected to pressure and thermal loading in terms of radial stress in the (a) inner pipe; (b) insulation and (c) outer pipe (d) von-Mises stress in the inner pipe; (e) von-Mises stress in the insulation and (f) von-Mises stress in the outer pipe – units in Pa.

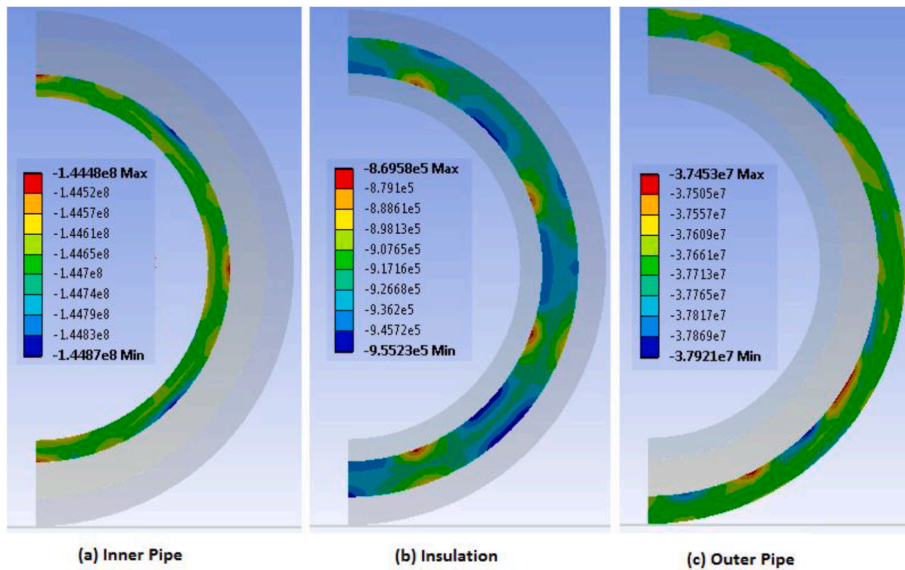
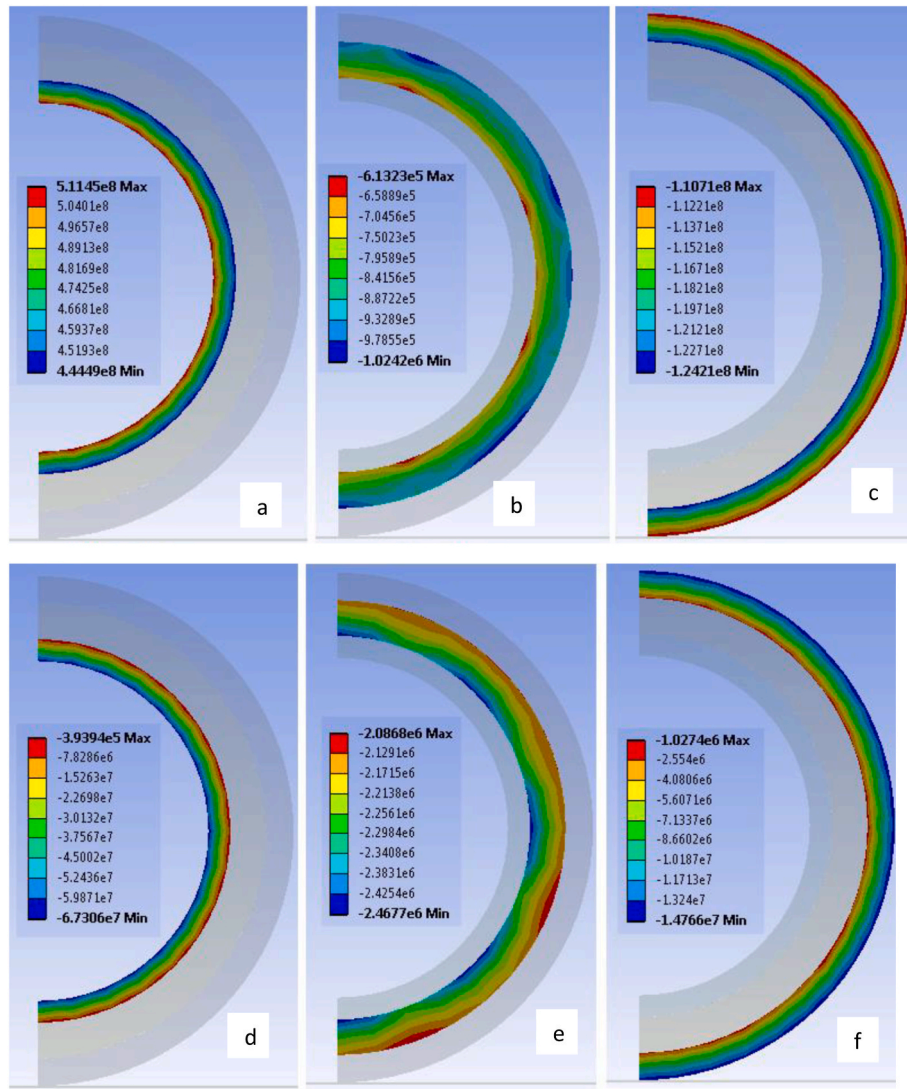


Fig. 15. FEA results for frictional pipe-in-pipe on a flat seabed, subjected to pressure and thermal loading in terms of axial stress in the (a) inner pipe; (b) insulation and (c) outer pipe – units in Pa.

this accounts of the difference in magnitude between the hoop stresses in the inner and outer pipes.

The radial stresses in the PIP system subjected to pressure loading

only, presented on Fig. 9(d–f). The analytical calculation assumes thin-wall pipes and therefore radial stress equal to zero (Harrison et al., 1997). However, the FEA shows that the true stress profile across the



**Fig. 16.** FEA results for frictional pipe-in-pipe on a flat seabed, subjected to pressure and thermal loading in terms of hoop stress in the (a) inner pipe; (b) insulation and (c) outer pipe (d) radial stress in the inner pipe; (e) radial stress in the insulation and (f) radial stress in the outer pipe – units in Pa.

thickness of the wall, this is insignificant on the inner surface of the inner pipe and the outer surface of the outer pipe. It should be noted that there are still relatively small radial stresses present on the outer surface of the inner pipe (67.79 MPa compressive) and the inner surface of the outer pipe (14.79 MPa compressive).

The von-Mises stresses are shown on Fig. 9(a–c), the von-Mises stress is greatest in the inner pipe as shown on Fig. 9(a). The stress profiles shown on Fig. 9 indicates that the inner surface of both the inner and outer pipes have the largest stress magnitude. This characteristic of the stress profiles is primarily due to the hoop stress, as the radial stresses are not significant, and the axial stress is uniform throughout the wall thickness.

It should be noted that in terms of all principal stresses and thus the von-Mises stress, there are no significant stresses present in the insulation material. This is because the stresses are carried through the inner and outer pipes. This study has revealed the load transfer mechanism and the quantitative values of the possible stresses that exist in the PIP system.

**5.5. Effect of thermal loading on PIP stresses: Frictionless condition**

In order to calculate the relevant stresses in the case of a frictionless pipe-in-pipe system subjected to thermal loading, the relevant

constraints are again applied, and simulation performed.

The axial and hoop stresses in the inner pipe, insulation and outer pipe are presented on Fig. 10 (a-f). It is clear that axial stress varies only slightly, in terms of the inner pipe, the variance is from  $-278.87$  MPa to  $-278.97$  MPa. The axial stress in the insulation varies from  $-0.133$  MPa to  $-0.155$  MPa and the outer pipe varies from  $0.85$  MPa to  $0.80$  MPa. Similarly, the hoop stresses computed are shown on Fig. 10(d), which shows that the hoop stress in the inner pipe varies from  $-3.153$  MPa at the outer surface to  $-3.743$  MPa at the inner surface. The hoop stress on the insulation is shown on Fig. 10(e), the hoop stress varies from  $-0.151$  MPa at the outer surface, to  $0.085$  MPa at the inner surface. On the outer pipe, hoop stress varies from  $3.17$  MPa to  $2.71$  MPa.

The radial stresses in the inner pipe vary from  $0.035$  MPa at the inner surface to  $-0.45$  MPa at the outer wall as shown on Fig. 11(a–c). Fig. 12 (a–c) presents the von-Mises stresses which appeared constant throughout the inner pipe with a value of  $277.15$  MPa. The von-Mises stress varies in the insulation from  $0.29$  MPa to  $0.19$  MPa and in the outer pipe, the maximum value is seen at the inner surface to be  $3.114$  MPa at the inner surface and  $2.40$  MPa at the outer surface.

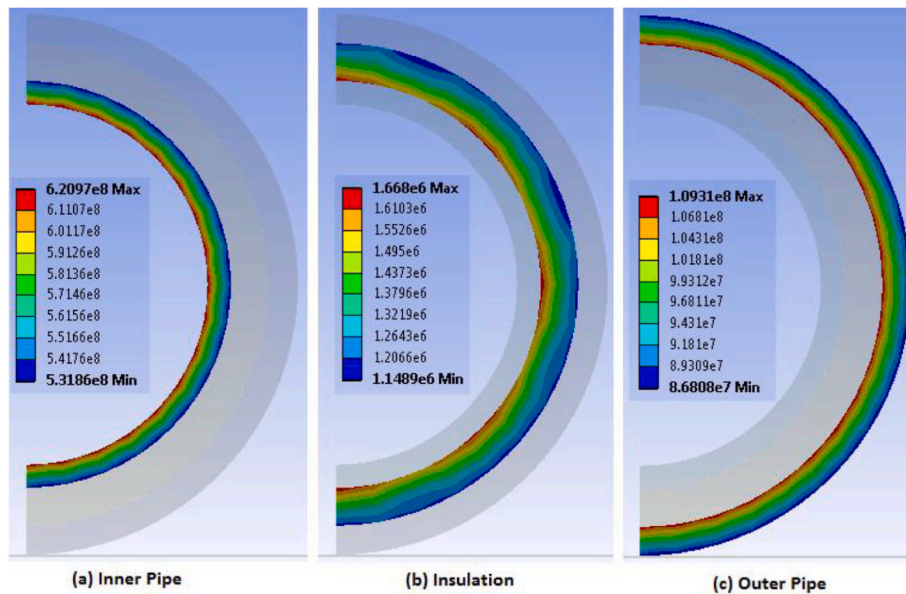


**Fig. 17.** FEA results for frictional pipe-in-pipe on a flat seabed, subjected to pressure and thermal loading in terms of von-Mises stress in the (a) inner pipe; (b) insulation and (c) outer pipe – units in Pa.

### 5.6. Effect of combined loading (pressure and temperature) on PIP stresses: Frictionless condition

In order to calculate the relevant stresses in the case of the frictionless pipe-in-pipe subjected to pressure and thermal loading are applied and simulation performed. It may be seen clearly in Fig. 13(a–c) that the axial stresses are approximately constant throughout the wall thicknesses of each body. The inner pipe varies from  $-142.23$  MPa to  $-142.53$  MPa; the insulation from  $-0.6$  MPa to  $-0.62$  MPa and in the outer pipe from  $-39.501$  MPa to  $-39.322$  MPa. Fundamentally, under the combined loading it is observed that the axial stress appears to be nonuniform owing to combined influence of the pressure and the temperature loading.

The contour plots of hoop stresses are presented in Fig. 13(d–f). The hoop stress in the inner pipe can be seen to vary from  $518.99$  MPa at the inner wall to  $450.91$  MPa at the outer wall of the inner pipe. The hoop stress in the insulation varies from  $-0.48$  MPa at the inner surface to  $-0.66$  MPa at the outer surface. As shown on Fig. 11(f) hoop stresses in the outer pipe varies from  $-116.51$  MPa to  $-130.57$  MPa at the outer and inner surfaces respectively.

Fig. 14 shows the radial stress through each body; it is clear from these results that the radial stress in the inner pipe ranges in values from  $0.622$  MPa to  $-67.28$  MPa Fig. 14(a). The radial stress in the insulation varies from  $-1.376$  MPa to  $-1.555$  MPa Fig. 14(b). The radial stress in the outer pipe varies from  $-0.634$  MPa at the inner surface to  $-14.783$  MPa at the outer surface. This is as shown on Fig. 14(c). The inner pipe has a value of von-Mises stress equal to  $627.17$  MPa at the inner surface and  $536.46$  MPa at the outer surface (Fig. 14(d)). In relation to the insulation, von-mises stress varies from  $0.76$  MPa at the outer surface to  $1.01$  MPa at the inner surface (Fig. 14(e)). Finally, Fig. 14(f) shows that the von-Mises stress in the outer pipe in this case varies from  $115.42$  MPa at the inner radius, to  $91.95$  MPa at the outer surface.

### 5.7. Effect of combined loading (pressure and temperature) on PIP stresses: Frictional condition

The above simulations are repeated considering frictional boundary conditions. The constraints of the model are the same as those used in the previous section described for frictionless analysis. The major difference is the contact settings whereby a frictional surface-to-surface

contact region between the outer surface of the outer pipe and the seabed, with a friction factor of  $0.4$  is utilised. Further, two frictional surface-to-surface contact regions are used between the outer/inner pipes and the insulation, these include a friction factor of  $0.3$ .

It can be seen on Fig. 15 that the axial stress profile is nonuniform through the wall thicknesses of each of the components, with values of  $-144.48$  MPa to  $-144.87$  in the inner pipe;  $-0.87$  MPa to  $-0.96$  MPa in the insulation material and in the outer pipe from  $-37.45$  MPa to  $-37.92$  MPa. This nonuniformity is more obvious under frictional condition than in frictionless condition of the seabed, revealing the complex load transfer between components of the PIP system and frictional force of the seabed. In addition, this nonuniform stress variation can induced degradation of the inner pipe, insulation and the outer pipe.

In terms of the hoop stress, it is shown on Fig. 16(a–c) and that the maximum in the inner pipe occurs at the inner surface, with a value of  $511.45$  MPa and the minimum at the outer surface at  $444.49$  MPa. The hoop stress in the insulation is relatively low with values from  $-0.613$  MPa to  $-1.02$  MPa. The hoop stress in the outer pipe is compressive throughout the wall thickness, the maximum of  $-124.21$  MPa occurs at the inner wall and the minimum of  $-110.71$  MPa occurs on the outer surface. The radial stress is shown on Fig. 16(d–f). It shows the radial stress in the inner pipe varies from  $-67.31$  MPa at the inner surface of the inner pipe to  $-0.394$  MPa at the outer surface. The radial stress in the insulation is approximately uniform throughout the wall thickness with values ranging from  $-2.09$  MPa to  $-2.47$  MPa. The radial stress at the inner surface of the outer pipe is  $-1.027$  MPa, this varies through the wall thickness to  $-14.76$  MPa at the outer surface.

The von-Mises stresses are presented on Fig. 17, it is shown that the von-Mises stress varies from  $620.97$  MPa at the inner surface of the inner pipe to  $531.86$  MPa at the outer surface. The von-Mises stress in the insulation is approximately uniform with values ranging from  $1.67$  MPa to  $1.15$  MPa. The von-Mises stress in the outer pipe varies from  $109.8$  MPa at the inner surface to  $86.81$  MPa at the outer surface.

### 5.8. Effect of load transfer between PIP and the seafloor

Keeping all parameters constant, another simulation was performed to determine the complex interaction between the PIP and the seafloor based on frictional and frictionless contacts. Contacts models capture how forces are transferred between two bodies. Interestingly, it was

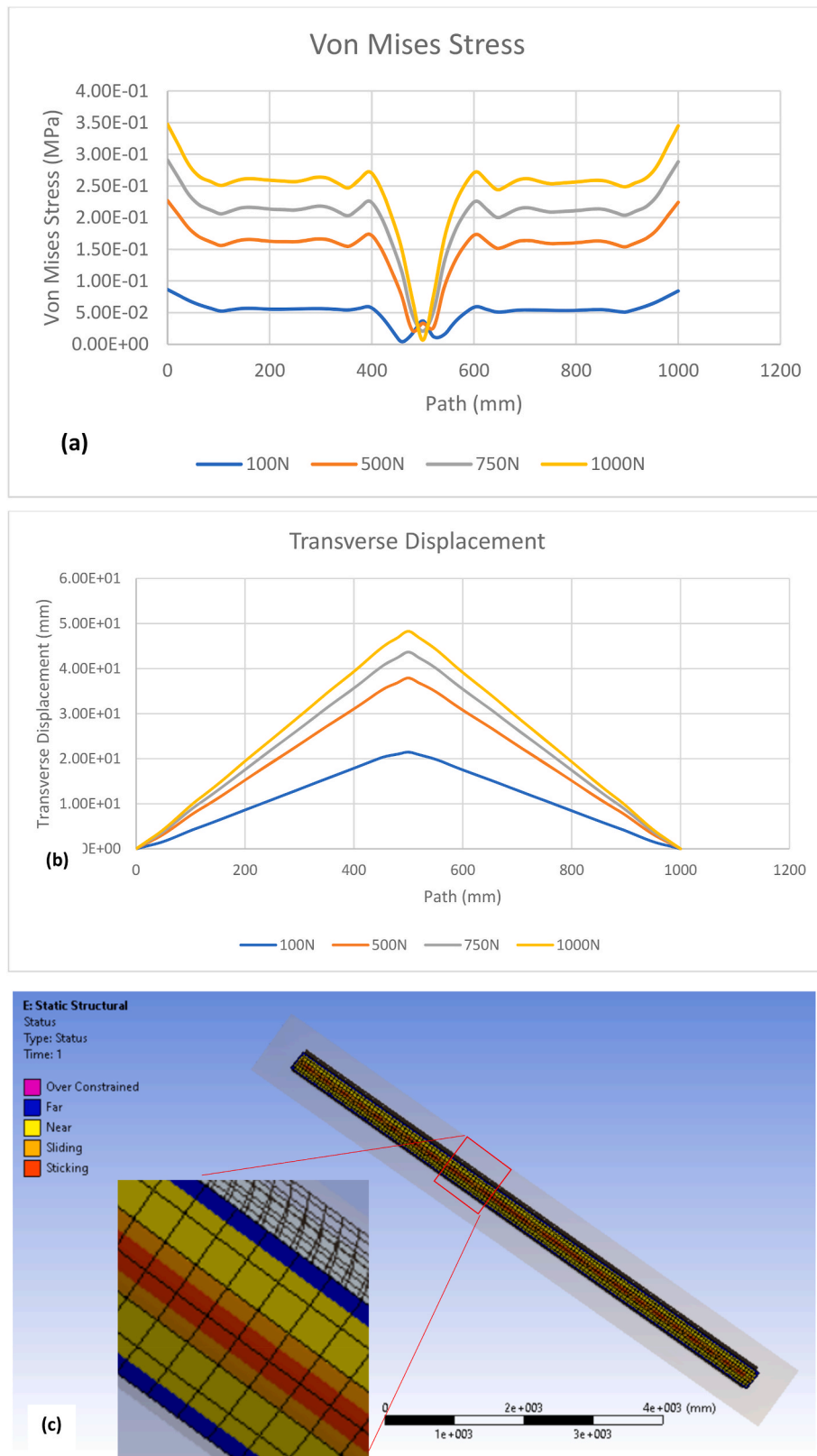


**Fig. 18.** (a) von Mises stress distribution on seafloor due to applied force (b) Transverse displacement on seafloor due to applied force (c) contact status between the seafloor and the PIP.

**Table 4**  
Summary of frictionless and frictional results.

	Frictionless		Frictional		Percentage Difference	
	Inner Pipe	Outer Pipe	Inner Pipe	Outer Pipe	Inner Pipe	Outer Pipe
Axial Stress (MPa)	-142.53	-39.50	-144.48	-37.92	1.35%	4%
Radial Stress (MPa)	-67.27	-14.78	-67.31	-14.76	0.06%	0.14%
Hoop Stress (MPa)	518.99	-130.57	511.41	-124.21	1.50%	4.80%
von Mises Stress (MPa)	627.17	115.42	620.97	109.31	0.98%	5.30%

found that transverse displacement between the PIP and the seafloor is similar for both frictional and the frictionless contacts based on the applied forces and the penalty and Lagrange formulations.

Fig. 18(a) present variation of the von Mises stress based on the load transfer between the PIP system and the seafloor. The maximum von Mises stress recorded is 0.3475 MPa and the minimum is 0.006559 MPa. In the same way, a similar trend is observed on the resulting transverse displacement as shown on Fig. 18(b). Again, the maximum transverse displacement is 48.27 mm at middle of (5000 mm) which correspond to the centre of gravity and the applied load of 1000N. Furthermore, the contact status revealed the complex interaction between the PIP and the seafloor showing the stick, sliding, near and far regions as shown on Fig. 18(c).

## 6. Conclusion

In conclusion, systematic study of pressure, temperature and the combination of both was successfully carried-out on the PIP system under 4700 ft of water. The results obtained from this study show the stresses developed on each component of the pipe-in-pipe system under different scenarios. As such, this study proved to provide new relevant knowledge on the load transfer mechanism in PIP system and the corresponding stress that is developed in the entire PIP structure in subsea water.

In summary, the investigation of nonlinear load transfer between inner pipe, insulation material, outer pipe and seabed are carried out under applied pressure loads, temperature and the combination of both. However, the study is limited to the 9m pipeline length, seabed conditions assumed, and internal and external pressure mimicking internal fluid pressure and external hydrostatic pressure equivalent to 4700 ft of water depth. In addition, this work assumed seabed temperature of 4.44 °C with a HPHT fluids temperature of 120.15 °C applied externally and internally accordingly.

In terms of applicability, findings can be applied to flexible pipe, subsea jumpers, flowlines to establish stress distribution at touch down during installation and to quantify the transverse displacement (embankment) of the subsea structures – especially subsea pipeline, risers and cables. Future work will examine variable pressure and temperature loading as well as impact of current and wave action of the sea on the overall load transfer mechanism in PIP system.

Table 4 FEA result comparison between frictionless and frictional analysis for axial, radial, hoop and von Mises stresses. As it can be seen, the two results correlate very well indicating similarity. This similarity is attributed to the surface-to-surface frictional contact between the PIP and the seabed. Based on this percentage difference, specifically for the inner pipe, it can be concluded that the inner pipe (carrier pipe) benefit low percentage differentials than the outer pipe under both frictional and frictionless simulation scenarios. Hence, making the PIP system a

preferred choice than the conventional single pipe for HPHT deep-water development.

The analytical calculations of the pipe in pipe computed the axial, hoop and von Mises stresses for inner and outer pipe. These results are in good agreement with the FEA results. For example, axial stress on the outer pipe under frictionless scenario was -39.5 MPa while the analytical is -40.2 MPa. Similarly hoop stress on the outer pipe for FEA is -130.57 MPa, on the other hand, analytical calculations gave a value of -134.7 MPa. Moreover, under frictional simulation scenario, the inner pipe has a von Mises stress of 620.97 MPa, the corresponding value for analytical calculation is 620.7 MPa. In addition, the von Mises stress on the outer pipe for FEA and analytical calculations is 109.31 MPa and 119.7 MPa respectively.

Stress analysis results also show that the carrier pipe get improved protection as the external hydrodynamic loads are eliminated by the outer pipe. Specifically, the hoop stress in the inner pipe is tensile and largest in the inner pipe; in the outer pipe however, the hoop stresses are compressive. This is because the hoop stresses in each pipe are due to the pressures acting on that pipe individually. The inner pipe is affected by the inner operating pressure, which accounts for the tensile hoop stress recorded in this pipe. This factor also causes the hoop stress to be greatest on the inner surface of the inner pipe, reducing through the wall thickness towards the outer surface. Knowing how this stress traverse through the thickness of each component of the PIP system is a remarkable new knowledge that can assist the evaluation of the structural performance of the PIP system. These new results would mitigate design failures associated with load transfer between the components of fully bonded compliant PIP system under pressure, temperature and the combined loading conditions as established in this study.

In the outer pipe, the external hydrostatic pressure, is significant, therefore the stress is compressive. Similarly, the hoop stress on the outer surface is considerably greater than on the inner surface. This is because of the hoop stress being affected by both the thermal and pressure loading. The operating pressure is greater than the hydrostatic pressure and this accounts for the difference in magnitude between the hoop stresses in the inner and outer pipes. Interestingly, both frictional and frictionless simulations results correlate very well, however, the nonuniform stress distribution is more obvious under frictional simulation scenario owing to frictional forces acting on the PIP system as established in the study. Based on this finding, material degradation will be more under frictional scenario than in frictionless condition of the seabed.

## CRedit authorship contribution statement

**Auwalu I. Mohammed:** Conceptualization, Data curation, Formal analysis, Investigation, Methodology, Software, Validation, Visualization, Writing – original draft, Writing – review & editing. **Konstantinos Bartzas:** Conceptualization, Data curation, Formal analysis, Investigation, Methodology, Software, Validation, Visualization, Writing – original draft, Writing – review & editing. **Callum Johnson:** Conceptualization, Data curation, Formal analysis, Investigation, Methodology, Software, Validation, Visualization, Writing – original draft, Writing – review & editing. **Stuart Spence:** Methodology, Conceptualization, Data curation, Formal analysis, Investigation, Software, Visualization, Writing – original draft, Writing – review & editing. **Paul Skyes:** Conceptualization, Data curation, Formal analysis, Investigation, Methodology, Software, Validation, Visualization, Writing – original draft, Writing – review & editing. **George Kidd:** Conceptualization, Data curation, Formal analysis, Investigation, Methodology, Supervision, Validation, Visualization, Writing – original draft, Writing – review & editing. **Jennifer McConnachie:** Conceptualization, Data curation, Formal analysis, Investigation, Methodology, Software, Supervision, Validation, Visualization, Writing – original draft, Writing – review & editing. **James Njuguna:** Conceptualization, Data curation, Formal analysis, Funding acquisition, Investigation, Methodology,

Project administration, Resources, Software, Supervision, Validation.

### Declaration of competing interest

The authors declare that they have no known competing financial interests or personal relationships that could have appeared to influence the work reported in this paper.

### Data availability

Data will be made available on request.

### References

- Adegboye, M.A., Fung, W.K., Karnik, A., 2019. Recent advances in pipeline monitoring and oil leakage detection technologies: principles and approaches. *Sensors* 19 (11), 2548.
- Auwalu, I.M., Zahra, I.Z., Adamu, M.B., Usman, A.L., Sulaiman, A.D., 2015. Effectiveness of simulations on well control during HPHT well drilling. In: *InSPE Nigeria Annual International Conference and Exhibition*. OnePetro.
- Bai, Q., Bai, Y., 2014. *Subsea Pipeline Design, Analysis, and Installation*. Gulf Professional Publishing.
- Bayart, C., Szyszka, T., Geertsen, D., 2007. Going into 2000m+ waters: are pipe-in-pipe getting too heavy installations?. In: *5th PetroMin Deepwater and Subsea Technology*.
- Bokaian, A., 2004. Thermal expansion of pipe-in-pipe systems. *Mar. Struct.* 17 (6), 475–500.
- Cai, J., Le Grogne, P., 2022. Lateral buckling of submarine pipelines under high temperature and high pressure—a literature review. *Ocean. Eng.* 244, 110254.
- Choi, H.S., 2001. Free spanning analysis of offshore pipelines. *Ocean. Eng.* 28 (10), 1325–1338.
- Chung, J.S., Cheng, B.R., 1996. Nonlinear coupled responses to impact loads on free-span pipeline: torsional coupling, load steps and boundary conditions. *Int. J. Offshore Polar Eng.* 6, 01.
- Chung, J.S., Cheng, B.R., Huttelmaier, H.P., 1995. Three-dimensional nonlinear responses to impact loads on free-span pipeline: torsional coupling and load steps. In: *InThe Fifth International Offshore and Polar Engineering Conference*. OnePetro.
- Deng, Y.S., Li, L., Yao, Z.G., Meng, L.Q., 2022. Stress intensity factors and fatigue crack growth law of cracked submarine special-shaped pipe under earthquake load. *Ocean. Eng.* 257, 111267.
- Dong, L., Zhang, Q., Huang, Y., Liu, G., 2017. Slip and stress of tensile armors in unbonded flexible pipes close to end fitting considering an exponentially decaying curvature distribution. *Mar. Struct.* 51, 110–133.
- Drafting, P., 2012. *Design*, by Roy A. Parisher and Robert A. Rhea.
- Gadala, I.M., Wahab, M.A., Alfantazi, A., 2016. Numerical simulations of soil physicochemistry and aeration influences on the external corrosion and cathodic protection design of buried pipeline steels. *Mater. Des.* 97, 287–299.
- Gao, X., Shao, Y., Chen, C., Zhu, H., Li, K., 2022. Experimental and numerical investigation on transverse impact resistance behaviour of pipe-in-pipe submarine pipelines after service time. *Ocean. Eng.* 248, 110868.
- Giagmouris, T., Tang, A., Qi, X., Zhong, J., 2013. Response and simulation of the pipe-in-pipe system in free spans. In: *InOffshore Technology Conference*. OnePetro.
- Guo, Y., Zhu, B., Zhao, X., Chen, B., Li, Y., 2020. Dynamic characteristics and stability of pipe-in-pipe system conveying two-phase flow in thermal environment. *Appl. Ocean Res.* 103, 102333.
- Harrison, G.E., Kerstenbaum, N.Y., Choi, H.S., 1997. Expansion analysis of subsea pipe-in-pipe flowline. In: *InThe Seventh International Offshore and Polar Engineering Conference*. OnePetro.
- Hausner, M., Dixon, M., 2004. Optimized design of pipe-in-pipe systems. *SPE Prod. Facil.* 19, 14–24, 01.
- Hong, Z., Liu, R., Liu, W., Yan, S., 2015. Study on lateral buckling characteristics of a submarine pipeline with a single arch symmetric initial imperfection. *Ocean. Eng.* 108, 21–32.
- Jones, R.L., Geertsen, C., Booth, P., Mair, J.A., Sriskandarajah, T., Rao, V., 2013. Pipe-in-pipe swaged field joint for reel lay. In: *InOffshore Technology Conference*. OnePetro.
- Jukes, P., Eltahir, A., Sun, J., 2009. The latest developments in the design and simulation of deepwater subsea oil and gas pipelines using FEA. In: *InThird ISOPE International Deep-Ocean Technology Symposium*. OnePetro.
- Kapuria, S., Salpekar, V.Y., Sengupta, S., 1999. Fatigue due to vortex-induced crossflow oscillations in free spanning pipelines supported on elastic soil bed. In: *InThe Ninth International Offshore and Polar Engineering Conference*. OnePetro.
- Kerstenbaum, N.Y., Harrison, G.E., Choi, H.S., 1996. Subsea pipeline lateral deviation due to high temperature product. In: *InThe Sixth International Offshore and Polar Engineering Conference*. OnePetro.
- Kong, D., Feng, L., Zhu, B., 2020. Assessment model of pipe–soil interaction during large-amplitude lateral displacements for deep-water pipelines. *Comput. Geotech.* 117, 103220.
- Kristoffersen, A.S., Askund, P.O., Nyström, P.R., 2012. Pipe-in-pipe global buckling and trawl design on uneven seabed. In: *InThe Twenty-Second International Offshore and Polar Engineering Conference*. OnePetro.
- Li, C., Liu, R., 2020. Numerical investigation into the effects of different initial imperfections on the lateral buckling of submarine pipelines. *Ocean. Eng.* 195, 106752.
- Liang, Z., Lu, X., Zhang, J., 2019. Thermal vertical buckling of surface-laid submarine pipelines on a sunken seabed. *Ocean. Eng.* 173, 331–344.
- Liao, M., Wang, G., Li, M., Zhao, Q., Gao, Z., 2022. Dynamics of an offshore drilling tube system with pipe-in-pipe structure based on drift element model. *Appl. Ocean Res.* 118, 102978.
- Mohammed, A.I., Oyeyeyin, B., Atchison, B., Njuguna, J., 2019. Casing structural integrity and failure modes in a range of well types-a review. *J. Nat. Gas Sci. Eng.* 68, 102898.
- Mohammed, A.I., Bartlett, M., Oyeyeyin, B., Kayvantash, K., Njuguna, J., 2021. An application of FEA and machine learning for the prediction and optimisation of casing buckling and deformation responses in shale gas wells in an in-situ operation. *J. Nat. Gas Sci. Eng.* 95, 104221.
- Mohammed, A.I., Bartlett, M., Oyeyeyin, B., Kayvantash, K., Njuguna, J., 2022. Multi-criteria material selection for casing pipe in shale gas wells application. *J. Pet. Explor. Prod. Technol.* 1–17.
- Odina, L., Hardjanto, F., Walker, A., 2018. Effects of impact loads on CRA-Lined pipelines. *Ocean Eng.* 166, 117–134.
- Palmer, A.C., Ling, M.T., 1981. Movements of submarine pipelines close to platforms. In: *InOffshore Technology Conference*. OnePetro.
- Park, H.I., Kim, C.H., 1997. Analytical methods for the determination of allowable free span lengths of subsea pipelines. In: *InThe Seventh International Offshore and Polar Engineering Conference*. OnePetro.
- Provasi, R., Toni, F.G., de Arruda Martins, C., 2022. Friction coefficient influence in a flexible pipe: a macroelement model. *Ocean. Eng.* 266, 112719.
- Rossini, N.S., Dassisti, M., Benyounis, K.Y., Olabi, A.G., 2012. Methods of measuring residual stresses in components. *Mater. Des.* 35, 572–588.
- Sriskandarajah, T., Anurudran, G., Ragupathy, P., Wilkins, R., 1999. Design considerations in the use of pipe-in-pipe systems for Hp/Ht subsea pipelines. In: *InThe Ninth International Offshore and Polar Engineering Conference*. OnePetro.
- Sun, J., Jukes, P., 2009. From installation to operation: a full-scale finite element modeling of deep-water pipe-in-pipe system. In: *InInternational Conference on Offshore Mechanics and Arctic Engineering*, vol. 43437, pp. 439–446.
- Sun, J., Jukes, P., Duan, G., 2009. Free span dynamics versus global buckling of the high pressure and high temperature pipeline. In: *InThe Nineteenth International Offshore and Polar Engineering Conference*. OnePetro.
- Sun, J., Jukes, P., Eltahir, A., 2009b. Exploring the challenges of pipe-in-pipe (PIP) flowline installation in deepwater. In: *InThird ISOPE International Deep-Ocean Technology Symposium*. OnePetro.
- Sun, J., Jukes, P., Wang, J., 2011. The Advancements of FEA in Confronting the Deepwater Pipelines under High Pressure and High Temperature. In: *OTC Brasil*, OnePetro.
- Sun, C., Zheng, M., Soares, C.G., Duan, M., Wang, Y., 2019. Theoretical prediction model for indentation of pipe-in-pipe structures. *Appl. Ocean Res.* 92, 101940.
- Trapper, P.A., 2022. A numerical model for geometrically nonlinear analysis of a pipe-lay on a rough seafloor. *Ocean. Eng.* 252, 111146.
- Veritas, D.N., 2006. *Free Spanning Pipelines*. Recommended Practice DNV-Rp105, pp. 1–46.
- Wang, H., Sun, J., Jukes, P., 2009. FEA of a laminate internal buckle arrestor for deep water pipe-in-pipe flowlines. In: *InInternational Conference on Offshore Mechanics and Arctic Engineering*, vol. 43437, pp. 447–452.
- Wang, Y., Qian, X., Liew, J.R., Zhang, M.H., 2014. Experimental behavior of cement filled pipe-in-pipe composite structures under transverse impact. *Int. J. Impact Eng.* 72, 1–16.
- Wang, Y., Zhang, X., Zhao, Y., Chen, H., Duan, M., Estefen, S.F., 2017. Perturbation analysis for upheaval buckling of imperfect buried pipelines based on nonlinear pipe-soil interaction. *Ocean. Eng.* 132, 92–100.
- Wang, Z., Duan, N., Soares, C.G., 2021. Controlled lateral buckling of subsea pipelines triggered by imposed residual initial imperfections. *Ocean. Eng.* 233, 109124.
- Watson, I., Walker, P., 2012. *Bundle Pipeline Systems and Shell FRAM Development*. Lunch and Learn with Shell and Subsea7, UK.
- Zhang, X., Duan, M., 2015. Prediction of the upheaval buckling critical force for imperfect submarine pipelines. *Ocean. Eng.* 109, 330–343.
- Zhang, J., Hu, T., 2022. Buckling failure mechanism of liner pipe in bimetal mechanical clad pipe under complex loading. *Ocean. Eng.* 262, 112091.
- Zhang, X., Duan, M., Soares, C.G., 2018. Lateral buckling critical force for submarine pipe-in-pipe pipelines. *Appl. Ocean Res.* 78, 99–109.
- Zheng, J., Palmer, A., Brunning, P., Gan, C.T., 2014. Indentation and external pressure on subsea single wall pipe and pipe-in-pipe. *Ocean Eng.* 83, 125–132.